https://doi.org/10.5194/acp-2021-723
Preprint. Discussion started: 23 September 2021

Atmospheric Chemistry and Physics Discussions

Exploration of the atmospheric chemistry of nitrous acid in a coastal city of southeastern China: Results from measurements across four seasons

Baoye Hu[1,2,3,4], Jun Duan[6], Youwei Hong[1,2], Lingling Xu[1,2], Mengren Li[1,2], Yahui Bian[1,2], Min Qin[6*], Wu Fang[6], Pinhua Xie[1,5,6,7], Jinsheng Chen[1,2*]

[1]Center for Excellence in Regional Atmospheric Environment, Institute of Urban Environment, Chinese Academy of Sciences, Xiamen 361021, China

[2]Key Lab of Urban Environment and Health, Institute of Urban Environment, Chinese Academy of Sciences, Xiamen 361021, China

[3]Fujian Provincial Key Laboratory of Pollution Monitoring and Control, Minnan Normal University, Zhangzhou, 363000, China

[4]Fujian Provincial Key Laboratory of Modern Analytical Science and Separation Technology, Minnan Normal University, Zhangzhou, 363000, China

[5]University of Chinese Academy of Sciences, Beijing 100086, China

[6]Key Laboratory of Environment Optics and Technology, Anhui Institute of Optics and Fine Mechanics, Chinese Academy of Sciences, Hefei, 230031, China

[7]School of Environmental Science and Optoelectronic Technology, University of Science and Technology of China, Hefei, 230026, China

Correspondence to: Jinsheng Chen (jschen@iue.ac.cn) &Min Qin (mqin@aiofm.ac.cn)

Abstract. Because nitrous acid (HONO) photolysis is a key source of hydroxyl (OH) radicals, identifying the atmospheric sources of HONO is essential to enhance the understanding of atmospheric chemistry processes and improve the accuracy of simulation models. We performed seasonal field observations of HONO in a coastal city of southeastern China, along with measurements of trace gases, aerosol compositions, photolysis rate constants (*J*), and meteorological parameters. The results showed that the average observed concentration of HONO was 0.54 ± 0.47 ppb. Vehicle exhaust emissions contributed an average of 1.64 % to HONO, higher than the values found in most other studies, suggesting an influence from diesel vehicle emissions. The mean conversion frequency of NO_2 to HONO in the nighttime was the highest in summer due to water

https://doi.org/10.5194/acp-2021-723
Preprint. Discussion started: 23 September 2021

Atmospheric Chemistry and Physics Discussions

droplets was evaporated under the condition of high temperatures. Based on a budget analysis, the rate of emission from unknown sources ($R_{unknown}$) was highest around midday, with values of 4.35 ppb·h^{-1} in summer, 3.53 ppb·h^{-1} in spring, 3.13 ppb·h^{-1} in autumn, and 2.05 in winter. Unknown sources made up the largest proportion of all sources in summer (78.55 %), autumn (71.51 %), spring (69.67 %), and winter (55.63 %). The photolysis of particulate nitrate was probably a source in spring and summer while the conversion from NO_2 to HONO on BC enhanced by light was perhaps a source in autumn and winter. The variation of HONO at night can be exactly simulated based on the HONO/NO_x ratio, while the $J(NO_3^-\_R) \times pNO_3^-$ should be considered for daytime simulations in summer and autumn, or $1/4\times(J(NO_3^-\_R) \times pNO_3^-)$ in spring and winter. Compared with O_3 photolysis, HONO photolysis has long been an important source of OH except for summer afternoon. Observation on HONO across four seasons with various auxiliary parameters improves the comprehension of HONO chemistry in southeastern coastal China.

1 Introduction

Nitrous acid (HONO) photolysis produces hydroxyl radical (OH), an important oxidant, in the troposphere (Zhou et al., 2011). OH plays an important role in triggering the oxidation of volatile organic compounds and therefore determine the fate of many anthropogenic atmospheric pollutants (Lei et al., 2018). Recent research results have shown that HONO production is the cause of an increase in secondary pollutants (Li et al., 2010; Gil et al., 2019; Fu et al., 2019). Though extensive studies have been conducted in the four decades since the first clear measurement of HONO (Perner and Platt, 1979), the HONO formation mechanisms are still elusive, especially during the daytime, when there is a large difference between measured concentrations and those calculated from known gas-phase chemistry (Sörgel et al., 2011a). Identification of the sources of atmospheric HONO and exploration of its formation mechanisms are beneficial for enhancing our comprehension of atmospheric chemistry processes and improving the accuracy of atmospheric simulation models.

Commonly accepted HONO sources include direct emission from motor vehicles (Chang et al., 2016; Kirchstetter et al., 1996; Kramer et al., 2020; Xu et al., 2015) or soil (Su et al., 2011; Tang et al., 2019; Oswald et al., 2013), the homogeneous conversion of NO by OH (Seinfeld and Pandis, 1998; Kleffmann, 2007), and the heterogeneous reaction of NO_2 on humid surfaces (Alicke, 2002; Finlayson-Pitts et al., 2003). Other homogeneous sources include nucleation reaction of NH_3, NO_2, and H_2O (Zhang and Tao, 2010), electronically excited H_2O and NO_2 for the production of HONO (Li et al., 2008), the $HO_2 \cdot H_2O$ complex and NO_2 for the production of HONO (Li et al., 2014). Other heterogeneous sources, include NO_2 reduced on soot to produce HONO and drastically enhanced by light(Ammann et al., 1998; Monge et al., 2010), semivolatile organics from diesel exhaust for the production of HONO (Gutzwiller et al., 2002), photoactivated of NO_2 on humic acid (Stemmler et al., 2006), TiO_2 (Ndour et al., 2008),solid organic compounds(George et al., 2005), the photolysis of particulate nitrate by ultraviolet (UV) light (Kasibhatla et al., 2018; Romer et al., 2018; Ye et al., 2017; Scharko et al., 2014), -dissolution of NO_2 catalyzed by anion on aqueous microdroplets (Yabushita et al., 2009), the process of acid displacement (Vandenboer et al., 2014), the conversion of NO_2 to HONO on the ground(Wong et al., 2011), NH_3 enhancing the

https://doi.org/10.5194/acp-2021-723
Preprint. Discussion started: 23 September 2021


Atmospheric Chemistry and Physics Discussions

heterogeneous reaction of NO_2 with SO_2 for the production of HONO (Ge et al., 2019), NH_3 promoting NO_2 dimers hydrolysis for HONO production through stabilizing the state of product and reducing the reaction free energy barrier (Li et al., 2018b; Xu et al., 2019), heterogeneous formation of HONO catalyzed by CO_2 (Xia et al., 2021). Heterogeneous processes are the most poorly understood, yet are widely considered the main sources of HONO in previous studies. The uptake coefficients of NO_2 conversion to HONO on surfaces (including aerosol, ground, buildings, and vegetation) vary from 10^{-9} to 10^{-2} derived from different experiments (Ammann et al., 1998; Kirchner et al., 2000; Underwood et al., 2001; Aubin and Abbatt, 2007; Zhou et al., 2015; Liu et al., 2014; Vandenboer et al., 2013). It is still a challenge to extrapolate laboratory results to real surfaces. It is still under exploration to distinguish the key step to determine the NO_2 uptake, and we are also not sure what role does radiation play in it. Absence of major HONO sources during the daytime is another active ongoing research.

According to an analysis of 15 sets of field observations around the world (Elshorbany et al., 2012), the HONO/NO_x ratio (0.02) predicts well HONO concentrations under different atmospheric conditions. To avoid underestimation of HONO in this study, an empirical parameterization was applied to estimating the HONO concentration, because the current understanding of HONO formation mechanisms is incomplete. Field measurements of HONO and its precursor NO_2 at sites with different aerosol load & composition, photolysis rate constants, and meteorological parameters are necessary to deepen our knowledge of the HONO formation mechanisms. Such measurements have been carried out in coastal cities in China, including Guangzhou (Qin et al., 2009), Hong Kong (Xu et al., 2015), and Shanghai (Cui et al., 2018), where the air pollution is relatively severe during their research period. However, there has been a lack of research into HONO in coastal cities with good air quality, low concentrations of $PM_{2.5}$, but strong sunlight and high humidity. Insufficient research on coastal cities with good air quality has resulted in certain obstacles to assessing the photochemical processes in these areas. Due to different emission-source intensities and ground surfaces, the atmospheric chemistry of HONO in the southeastern coastal area of China is predicted to have different pollution characteristics from those found in other coastal cities. Furthermore, HONO contributes to the atmospheric photochemistry differently depending on the season (Li et al., 2010). Therefore, observations of atmospheric HONO across different seasons in the southeastern coastal area of China are urgently needed.

Incoherent broadband cavity-enhanced absorption spectroscopy (IBBCEAS) was employed in this study to determine HONO concentrations in the southeastern coastal city of Xiamen in August (summer), October (autumn), and December (winter) 2018 and March (spring) 2019. In addition, a series of other relevant trace gases, meteorological parameters, and photolysis rate constants were measured at the same time to provide supplementary information to reveal the HONO formation mechanisms. The main purposes of this study were to (1) calculate the values of unknown HONO daytime sources, (2) analyze the processes leading to HONO formation, (3) simulate HONO concentrations based on an empirical parameterization, and (4) evaluate OH production from HONO from 07:00 to 16:00 local time. These results were compared between the seasons.

https://doi.org/10.5194/acp-2021-723
Preprint. Discussion started: 23 September 2021


Atmospheric Chemistry and Physics Discussions

2 Methodology

2.1 Site description

Our field observations were carried out ~80 m above the ground at a supersite located on the top of the Administrative Building of the Institute of Urban Environment (IUE), Chinese Academy of Sciences (118°04′13″E, 24°36′52″N) in Xiamen, China in August, October, and December 2018, and March 2019 (Fig. 1). The supersite was equipped with a complete set of measurement tools, including those for measuring gas and aerosol species composition, meteorology parameters, and photolysis rate constants, which provided a good chance to study the atmospheric chemistry of HONO in a coastal city of southeastern China. As shown in Fig. 1 (left), Xiamen is located at the southeast coastal area of China and faces the Taiwan Strait in the east. It suffers from sea and land breeze throughout the year with spring and summer more frequently (Xun et al., 2017). The IUE supersite is surrounded by a Xinglin Bay, several universities (or institutes), and several major roads with large traffic fleet, such as Jimei Road, Shenhai Expressway (870 m) and Xiasha Expressway (2300 m) (Fig. 1 (right)). The area of Xiamen is 1700.61 km^2 with a population of 4.11 million (http://tjj.xm.gov.cn/tjzl/). The number of motor vehicles in 2018 was 1,572,088, which was 2.73 times as many as ten years ago. The surrounding soil is used for green not for agriculture.

2.2 Instrumentation

The atmospheric concentrations of both HONO and NO_2 were determined using IBBCEAS, which has previously been widely applied to such measurements (Tang et al., 2019; Duan et al., 2018; Min et al., 2016). The IBBCEAS instrument was customized by the Anhui Institute of Optics and Fine Mechanic (AIOFM), Chinese Academy of Sciences (Duan et al., 2018). The resonant cavity is composed of a pair of high reflective mirrors separated by 70 cm and their reflectivity is approximately 0.99983 at 368.2 nm. The surface of the mirrors was purged by dry nitrogen at 0.1 Standard Liter per Minute (SLM), and the air flow was controlled by mass flow controller to prevent the surface of the mirror from being contaminated. Light was introduced into the resonant cavity and was emitted by a single light-emitting diode (LED) with full width at half maximum (FWHM) of 13 nm, peak wavelength of 365 nm. Light transmitted through the cavity was received by an QE65000 spectrometer (Ocean Optics) through an optical fiber with 600 μm diameter and a 0.22 numerical aperture.

In order to avoid the drift of the center wavelength of the LED, the temperature of the LED was controlled to be approximately 25 ± 0.01 °C by using a thermoelectric cooler unit. In order to prevent particulate matter from entering the cavity and reducing the effect of particulate matter on the effective absorption path, a 1 μm polytetrafluoroethylene (PTFE) filter membrane (Tisch Scientific) was used in the front end of the sampling port. In order to ensure the quality of the data, the 1 μm PTFE filter membrane was usually replaced once every three days and the sampling tube was thoroughly cleaned with alcohol once a month. We increased the replacement frequency of the filter membrane and the cleaning frequency of the sampling tube in the event of heavy pollution to ensure that the filter membrane and sampling tube are in a clean state.

https://doi.org/10.5194/acp-2021-723
Preprint. Discussion started: 23 September 2021


Atmospheric Chemistry and Physics Discussions

The length of sampling tube with 6 mm outer diameter was approximately 3 m, the material was PFA with excellent chemical inertness and the sampling flow rate was 6 SLM meaning that the residence time of the gas in the sampling tube was less than 0.5 s. Besides, the sampling loss was calibrated before the experiment. We assessed the measured spectrum every day to ensure the authenticity of the measurement results. Multiple reflections in the resonator cavity enhanced the length of the effective absorption path, thereby enhancing the detection sensitivity of the instrument. The 1σ detection limits for HONO and NO_2 were about 60 ppt and 100 ppt, respectively, and the time resolution was 1 min. The fitting wavelength range was selected as 359–387 nm. The measurement error of HONO of IBBCEAS was estimated to be about 9 %, considering both HONO secondary formation and sample loss. The sampling tube was heated to 35 °C and covered by insulation cotton materials to prevent the effect of condensation of the water vapor(Lee et al., 2013).

The inorganic composition of $PM_{2.5}$ aerosols (SO_4^{2-}, NO_3^-, Cl^-, Na^+, NH_4^+, K^+, Ca^{2+}, and Mg^{2+}) and concentrations of gases (HONO, HNO_3, HCl, SO_2, NH_3) were determined using a Monitor for AeRosols and Gases in ambient Air (MARGA, Model ADI 2080, Applikon Analytical B.V., the Netherlands). Ambient air was drawn into the sample box by a $PM_{2.5}$ cyclone (Teflon coated, URG-2000-30ENB) at the flow rate of 1 $m^3 \cdot h^{-1}$. Air sample was drawn firstly through the Wet Rotating Denuder (WRD) where gases diffused to the solution, and then particles were collected by a Steam Jet Aerosol Collector (SJAC). Absorption solutions were drawn from the SJAC and the WRD to syringes (25 ml). Samples were injected to Metrohm cation (500 µl loop) and anion (250 µl loop) chromatographs with the internal standard (LiBr) for 15 min after an hour when the syringes had been filled (Makkonen et al., 2012). Specific descriptions of the SJAC can be found in previous reports (Slanina et al., 2001; Wyers et al., 1993). Therefore, the times needed for the sampling period and the latter IC analysis on the MARGA system are a full hour and 15 minutes, respectively. The value measured in this hour is actual the concentration sampled in the previous hour, so the time corresponding to the sampling is matched with other instrument parameters (i.e., HONO, NO*x*, *J* values).

Photolysis frequencies were determined using a photolysis spectrometer (PFS-100, Focused Photonics Inc., Hangzhou, China). These were calculated by multiplying the actinic flux *F*, quantum yield $\varphi(\lambda)$ and the known absorption cross section $\sigma(\varphi)$. The measurements included the photolysis rate constants *J* (O^1D), *J* (HCHO_M), *J* (HCHO_R), *J* (NO_2), *J* (H_2O_2), *J* (HONO), *J* (NO_3_M) and *J* (NO_3_R), and the spectral band ranged from 270 to 790 nm. Hemispherical (2π sr) angular response deviations were within ±5 %. The photolysis rate constants with _R and _M represented radical photolysis channel and molecular photolysis channel, respectively. Specifically, HCHO was removed by the reactions (R1) and (R2), and NO_3 was removed by the reactions R(3) and R(4), respectively (Röckmann et al., 2010).

$$HCHO + h\nu \longrightarrow CHO + H \qquad J(HCHO\_R) \qquad \text{(R1)}$$

$$HCHO + h\nu \longrightarrow H_2 + CO \qquad J(HCHO\_M) \qquad \text{(R2)}$$

$$NO_3 + h\nu \longrightarrow NO_2 + O^3P \qquad J(NO_3\_R) \qquad \text{(R3)}$$

https://doi.org/10.5194/acp-2021-723
Preprint. Discussion started: 23 September 2021

Atmospheric Chemistry and Physics Discussions

157 $NO_3 + hv \longrightarrow NO + O_2$ $J(NO_3\_M)$ (R4)

158 The O_3 concentration was determined by UV photometric analysis [Model 49*i*, Thermo Environmental Instruments (TEI)
159 Inc.], and the detection limit of the TEI Model 49*i* is 1.0 ppb. The NO concentration was determined by a
160 chemiluminescence analyzer (TEI model 42*i*) with a molybdenum converter. The detection limit and the uncertainty of the
161 TEI model 42*i* were 0.5 ppb and 10 %, respectively. Although the TEI model 42*i* also measures the concentration of NO_2,
162 this value might actually include other active nitrogen components(Villena et al., 2012). As expected, the NO_2 concentration
163 measured by IBBCEAS had the same trend as the NO_2 measured by TEI 42*i*, and NO_2 concentration measured by IBBCEAS
164 was always lower than that by TEI 42i (Fig. S1). Therefore, the NO_2 concentration as measured by IBBCEAS was used in
165 this study. An oscillating microbalance with a tapered element was applied to determine the $PM_{2.5}$ concentration with
166 uncertainty of 10-20 %. Black carbon (BC) was measured by aethalometer at 7 wavelengths (in using 880 nm wavelength).
167 When the tape was < 10 %, aethalometer fiber tape was replaced. Meteorological parameters were determined by an
168 ultrasonic atmospherium (150WX, Airmar, USA). The time resolution of all instruments was unified to 1 h to facilitate
169 comparison. Ultraviolet radiation (UV) was determined by a UV radiometer (KIPP & ZONEN, SUV5 Smart UV
170 Radiometer).

171 **3 Results and discussion**

172 **3.1 Overview of data**

173 Figure 2 showed an overview of the determined HONO, NO, NO_2, $PM_{2.5}$, NO_3^-, BC, *J*(HONO), temperature (T) and relative
174 humidity (RH)in this study. The entire campaign was characterized by subtropical monsoon climate with high temperature
175 (9.82−34.42 °C) and high humidity (29.24−100 %). The mean values (± standard deviation) of temperature and relative
176 humidity were 22.24 ± 5.41 °C and 78.35 ± 14.07 %, respectively. Elevated concentrations of NOx, i.e., up to 156.17 ppb of
177 NO, and 172.42 ppb of NO_2, were observed, possibly due to dense vehicle emissions near this site. The photolysis rate
178 constants $J(O^1D)$, *J*(HCHO_M), *J*(HCHO_R), $J(NO_2)$, $J(H_2O_2)$, *J*(HONO), $J(NO_3\_M)$ and $J(NO_3\_R)$ had the same temporal
179 variation (Fig. S2), although their orders of magnitude were different. The correlation coefficients between *J*(HONO) and
180 other photolysis rate constants were above 0.965 (not shown). Both *J*(HONO) and UV peaked around noon, and the
181 maximum of *J*(HONO) (2.02×10^{-3} s^{-1}) and UV (55.62 $W\cdot m^{-2}$) appeared at 13:00 on 11 March 2019, and 12:00 on 14 August
182 2018, respectively. This area was dominated by photochemical pollution, while particulate pollution was relatively light., No
183 haze episodes occurred across four seasons with 111 days because daily mass concentration of $PM_{2.5}$ was lower than the
184 National Ambient Air Quality Standard (Class II: 75 $\mu g\cdot m^{-3}$). For O_3, 10 episodes occurred with eight-hour maximum
185 concentrations of O_3 exceeding the Class II: 160 $\mu g\cdot m^{-3}$. Maximum mixing ratio of O_3 was 113.81 ppb, occurring in the
186 afternoon with strong ultraviolet radiation (42.72 $w\cdot m^{-2}$) and low NO concentration (0.75 ppb) titrating O_3. In general, the
187 level of pollutants in this area was relatively low. Campaign-averaged levels of NO_2, NO, NO_3^-, $PM_{2.5}$, O_3, and BC were

https://doi.org/10.5194/acp-2021-723
Preprint. Discussion started: 23 September 2021


Atmospheric Chemistry and Physics Discussions

188 14.99 ± 8.93 ppb, 5.80 ± 11.98 ppb, 5.59 ± 6.26 μg·m^{-3}, 27.78 ± 17.95 μg·m^{-3}, 28.29 ± 21.14 ppb, and 1.67 ± 0.97 μg·m^{-3},
189 respectively. The maximum value of HONO (3.51 ppb) appeared at 08:00 on 4 December 2018. The high value of HONO
190 was always accompanied by relative high values of NO and NO_2 or $PM_{2.5}$, BC and NO_3^-. The average measured ambient
191 HONO concentration at the measurement site for all measurement periods was 0.54 ± 0.47 ppb. The HONO concentration
192 measured at this site was comparable to those measured at other suburban sites (Liu et al., 2019c; Xu et al., 2015; Nie et al.,
193 2015a; Park et al., 2004), was obvious lower than those measured at urban sites and industrial site (Li et al., 2018a; Yu et al.,
194 2009; Hou et al., 2016; Qin et al., 2009; Wang et al., 2013; Shi et al., 2020; Spataro et al., 2013; Huang et al., 2017; Wang et
195 al., 2017), and was obvious higher than those measured at marine background(Wen et al., 2019a), Marine boundary layer(Ye
196 et al., 2016), and coastal remote (Meusel et al., 2016) , as shown in Table S1.

197 As shown in Table 1, in the daytime (06:00–18:00, including 06:00, local time (LT)), the highest concentration of HONO
198 was found in spring and summer (0.72 ppb), followed by winter (0.61 ppb) and autumn (0.50 ppb). In short, the seasonal
199 variation of HONO was well correlated with the seasonality of RH, with high RH in spring (84.21 %) and summer (84.12 %),
200 followed by winter (78.13 %) and autumn (69.55 %). In conditions of low RH, the adsorption rate of NO_2 is not as rapid as
201 that of HONO, resulting in a reduction in the conversion rate of NO_2 to HONO and thus a reduction in the concentration of
202 HONO (Stutz et al., 2004). This seasonal variation in HONO concentration was different from those measured in Jinan (Li et
203 al., 2018a), Nanjing (Liu et al., 2019b), and Hong Kong (Xu et al., 2015). The elevated HONO concentrations in summer,
204 when there is strong solar radiation, suggests the existence of strong sources of HONO and its important contribution to the
205 production of OH radicals. Interestingly, the HONO concentration in the nighttime was lower than that in the daytime in all
206 four seasons. Most previous studies have found that the HONO concentration at night is significantly higher than that during
207 the day (Wang et al., 2015; Liu et al., 2019c; Li et al., 2018a; Elshorbany et al., 2009; Acker et al., 2006; Yu et al., 2009).
208 Coastal cities are susceptible to sea and land breezes, with sea breezes blowing during the day and land breezes blowing
209 during the night (Wagner et al., 2012). Therefore, the concentration of sea salt, as calculated based a previous report (Liu et
210 al., 2020), is significantly higher during the day (2.91 μg·m^{-3}) than that during the night (2.73 μg·m^{-3}) ($P < 0.05$). It is
211 possible that significantly more HONO could be produced by photolysis of sea salts against the daytime photolysis of
212 HONO (Kasibhatla et al., 2018). Similar results were found in Hong Kong, which is also a coastal city, which further
213 validates the rationality of this assumption (Xu et al., 2015). As shown in Fig. 3, larger difference between daytime and
214 nighttime HONO concentrations was observed on days with SLBs compared without SLBs, which indicated that SLBs did
215 cause higher HONO concentration in the daytime than that in the nighttime.

216 The ratio of HONO to NO_x or the ratio of HONO to NO_2 have been extensively applied to indicate heterogeneous conversion
217 of NO_2 to HONO (Li et al., 2012b; Liu et al., 2019c; Zheng et al., 2020). Compared with the HONO/NO_2 ratio, the
218 HONO/NO_x ratio can better avoid the influence of primary emissions (Liu et al., 2019c). In this study, the HONO/NO_x ratios
219 during the day were higher than those during the night, indicating that light promotes the conversion of NO_x to HONO. The
220 highest daytime HONO/NO_x ratio was found in summer (0.072), followed in turn by autumn (0.048), spring (0.034), and

https://doi.org/10.5194/acp-2021-723
Preprint. Discussion started: 23 September 2021


Atmospheric Chemistry and Physics Discussions

221 winter (0.023). The elevated HONO/NO_x ratio in summer indicates a greater net HONO production (Xu et al., 2015). The
222 low HONO/NO_x ratio in winter can probably be ascribed to heavy emissions and high concentrations of NO in winter
223 (Table 1). The HONO/NO_x ratios during every season in Xiamen were in general higher than those found in studies of other
224 cities, which indicates greater net HONO production in Xiamen.

225 The diurnal patterns of HONO, NO_x, HONO/NO_x, and $J(NO_2)$ averaged for every hour in each season are shown in Fig. 4.
226 As shown in Fig. 4a, the HONO concentration had similar diurnal variation patterns across the four seasons. The maximum
227 values of the HONO concentration were 1.12 ppb in winter, 1.03 ppb in summer, 0.98 ppb in spring, and 0.65 ppb in autumn,
228 and these occurred in the morning rush hour (07:00–08:00), which indicates that direct vehicle emissions may be a
229 significant source of HONO. The contribution of direct vehicle emissions to HONO will be quantified in Sect. 3.2. The
230 HONO concentration reduced rapidly from the morning rush hour to sunset, and this was caused by rapid photolysis
231 combined with increased height of the boundary layer. The minimum values of HONO concentration were 0.47 ppb in
232 spring, 0.23 ppb in winter, 0.21 ppb in summer, and 0.14 ppb in autumn, and these appeared at sunset, between 16:00 and
233 18:00. The HONO concentration increased gradually after sunset, which indicates that release from HONO sources exceeded
234 its dry deposition (Wang et al., 2017). There was a slight difference in the diurnal variation of HONO between autumn and
235 the other seasons. A rapid reduction of HONO after the morning rush hour was found in spring, summer, and winter. In
236 comparison, the HONO in autumn had an almost constant concentration between 07:00 and 11:00 because NO_x decreased
237 slowly during this period.

238 As shown in Fig. 4b, NO_x concentration followed an expected profile in the four seasons, with peaks of 45.58 ppb in winter,
239 40.47 ppb in spring, 32.47 ppb in summer, and 20.07 ppb in autumn, each occurring in the morning rush hour at 10:00, 09:00,
240 08:00, and 07:00 local time, respectively. After these peaks, NO_x decreased during the day in each season, probably due to
241 photochemical transformation and increasing boundary-layer depth. The NO_x concentrations then began to rise from their
242 minima of 8.20 ppb in summer, 8.85 ppb in autumn, 18.10 ppb in winter, and 23.09 ppb in spring after 14:00, 13:00, 15:00,
243 and 16:00 local time, respectively, which was caused by a combination of weak photochemical transformation and reduction
244 in the boundary-layer depth. The NO_x concentrations during winter and spring were significantly higher than those during
245 autumn and summer. Both the maxima and minima of NO_x appeared later in spring and winter compared with summer and
246 autumn.

247 It is possible to better describe the behavior of HONO using the HONO/NO_x ratio. The higher HONO/NO_x ratio found at
248 noon in the different seasons, especially in summer and autumn (Fig. 4c), indicates an additional daytime HONO source(Liu
249 et al., 2019c; Xu et al., 2015). It is worth noting that the maximum value of this ratio in summer (0.147) was significantly
250 higher than the maximum in other seasons, especially in winter (0.034). Fig. 4d shows that the value of the HONO/NO_x ratio
251 increased with the photolysis of NO_2 in summer and autumn, suggesting that the additional HONO source is probably
252 correlated with light (Xu et al., 2015; Wang et al., 2017; Li et al., 2018a; Li et al., 2012b). The increase in the HONO/NO_2
253 ratio during the day can be seen more clearly in Fig. 5, and its high value indicates a high HONO production efficiency,

https://doi.org/10.5194/acp-2021-723
Preprint. Discussion started: 23 September 2021


Atmospheric Chemistry and Physics Discussions

254 which cannot be ascribed to NO_2 conversion due to the weak correspondence between HONO and NO_2 in in summer.
255 Furthermore, high HONO/NO_2 ratios were accompanied by high $J(NO_2)$ in summer, which indicates that HONO formation
256 during the daytime is controlled by light rather than Reaction (R5).

257 $$NO_2 + NO_2 + H_2O \xrightarrow{surf} HONO + HNO_3 \quad (R5)$$

258 However, the observed maxima can also be ascribed to sources independent from NO_x concentration, such as soil emissions
259 (Su et al., 2011) and photolysis of particulate nitrate (Zhou et al., 2011; Ye et al., 2016), which are not influenced by the
260 decrease of NO_x concentration around noon. A more specific discussion of daytime HONO sources considering the
261 photolysis of particulate nitrate will be given in Sect. 3.4.3. The HONO emissions from soil were estimated to be 2–5 ppb h^{-1}
262 (Su et al., 2011). However, soil emission was a negligible source of HONO in this study since the surrounding soil is not
263 used for agriculture, and this greatly reduces the amount of HONO released due to no fertilization process (Su et al., 2011).

264 **3.2 Direct vehicle emission of HONO**

265 The K^+ levels were 0.26, 0.13, 0.14, and 0.24 $\mu g \cdot m^{-3}$ for spring, summer, autumn, and winter, respectively. The K^+ levels
266 during the four seasons were lower than 2 $\mu g \cdot m^{-3}$, which indicated that biomass burning has little effect on this site (Nie et al.,
267 2015b; Xu et al., 2019). Hence, only vehicle emissions were considered in this study. The consistent diurnal variations in
268 HONO and NO_x presented in Sect. 3.1 (Fig. 4) also indicate HONO emissions from local traffic. Five criteria were applied to
269 choose cases that guaranteed the presence of fresh plumes (Xu et al., 2015; Liu et al., 2019c): (1) UV < 10 $W \cdot m^{-2}$; (2) short-
270 duration air masses (<2 h); (3) HONO correlating well with NO_x ($R^2 > 0.60$, $P < 0.05$); (4) NO_x > 20 ppb (highest 25 % of
271 NO_x value); and (5) NO/NO_x > 0.50. A total of 34 cases met these strict criteria for estimation of the HONO vehicle
272 emission ratios. The slopes of scatter plots of HONO vs NO_x were used as the emission factors.

273 A total of 34 vehicle emission plumes were summarized in Table 2, and these were used for estimation of the vehicle
274 emission ratios. These plumes were considered to be truly fresh because the mean $\Delta NO/\Delta NO_x$ ratio of the selected air masses
275 was 92 %. Vehicle plumes unavoidably mixing with other air masses resulted in the correlation coefficients (R^2) between
276 HONO and NO_x varying among the cases, and these ranged from 0.61to 0.92. The obtained $\Delta HONO/\Delta NO_x$ ratios ranged
277 from 0.24 % to 4.76 %, with an average value (±SD) of (1.64 ± 0.95) %. These $\Delta HONO/\Delta NO_x$ ratios have comparability to
278 those obtained in Guangzhou (1.4 % (Qin et al., 2009); 1.8 % (Li et al., 2012b)) and Houston (1.7 % (Rappenglück et al.,
279 2013)), but are significantly higher than those measured in Jinan (0.53 % (Li et al., 2018a)) and Santiago (0.8 % (Elshorbany
280 et al., 2009)). The types of vehicle engine, the use of catalytic converters, and different fuels will affect the vehicle emission
281 factors (Kurtenbacha et al., 2001). A potential reason for the relatively higher $\Delta HONO/\Delta NO_x$ values in our study is that
282 heavy-duty diesel vehicles pass by on the surrounding highway (Rappenglück et al., 2013). It is necessary to examine the
283 specific vehicle emission factors in target cities because of these differences in $\Delta HONO/\Delta NO_x$ ratios. Roughly assuming that

https://doi.org/10.5194/acp-2021-723
Preprint. Discussion started: 23 September 2021

Atmospheric Chemistry and Physics Discussions

NO_x mainly arises from vehicle emissions, a mean $\Delta HONO/\Delta NO_x$ value of 1.64 % was used as the emission factor in this study, and this value was adopted to estimate the contribution of vehicle emissions P_{emis} to the HONO concentration using

$$P_{\text{emis}} = \text{NO}_x \times 0.0164. \quad (1)$$

We can then obtain the corrected HONO concentration ($HONO_{corr}$) for further analysis from the equation

$$\text{HONO}_{\text{corr}} = \text{HONO} - P_{\text{emis}}. \quad (2)$$

3.3 Nighttime heterogeneous conversion of NO_2 to HONO

3.3.1 Conversion rate of NO_2 to HONO

Nighttime $HONO_{corr}$ concentrations can be estimated from the heterogeneous conversion reaction (Meusel et al., 2016; Alicke, 2002; Su et al., 2008c). Although the mechanism of the nighttime HONO heterogeneous reaction is unclear, the formula for the heterogeneous conversion (C^0_{HONO}) of NO_2 to HONO can be expressed as

$$C^0_{\text{HONO}} = \frac{[\text{HONO}_{\text{corr}}]_{t_2} - [\text{HONO}_{\text{corr}}]_{t_1}}{(t_2 - t_1) \times \overline{[\text{NO}_2]}}, \quad (3)$$

where $\overline{[\text{NO}_2]}$ is the mean value of NO_2 concentration between t_1 and t_2. Eq. (4) has been suggested as a way to avoid the interference of direct emissions and diffusion (Su et al., 2008c):

$$C^X_{\text{HONO}} = \frac{\left(\frac{[\text{HONO}_{\text{corr}}]_{(t_2)}}{[X]_{t_2}} - \frac{[\text{HONO}_{\text{corr}}]_{(t_1)}}{[X]_{(t_1)}}\right)\overline{[X]}}{(t_2 - t_1)\frac{1}{2}\left(\frac{[\text{NO}_2]_{(t_2)}}{[X]_{(t_2)}} + \frac{[\text{NO}_2]_{(t_1)}}{[X]_{(t_1)}}\right)\overline{[X]}} = \frac{2\left(\frac{[\text{HONO}_{\text{corr}}]_{(t_2)}}{[X]_{t_2}} - \frac{[\text{HONO}_{\text{corr}}]_{(t_1)}}{[X]_{(t_1)}}\right)}{(t_2 - t_1)\left(\frac{[\text{NO}_2]_{(t_2)}}{[X]_{(t_2)}} + \frac{[\text{NO}_2]_{(t_1)}}{[X]_{(t_1)}}\right)}, \quad (4)$$

where $[\text{HONO}_{\text{corr}}]_t$, $[\text{NO}_2]_t$, and $[X]_t$ were the concentrations of HONO, NO_2, and species used for normalization (including NO_2, CO, and black carbon (BC) in this study), respectively, at time t, $\overline{X}$ is the average concentration of reference species between t_1 and t_2, and C^X_{HONO} represents the conversion rate normalized against reference species X (Su et al., 2008c). There were 91 cases meeting the criteria. Such a large number of cases contributes to the statistical analysis of the heterogeneity of HONO formation. The average values of C^0_{HONO}, $C^{\text{NO}_2}_{\text{HONO}}$, $C^{\text{CO}}_{\text{HONO}}$, and $C^{\text{BC}}_{\text{HONO}}$ were 0.48 % h^{-1}, 0.46 % h^{-1}, 0.47 % h^{-1}, and 0.46 % h^{-1}, respectively. The combined $C^{\text{C}}_{\text{HONO}}$ was 0.47 % h^{-1}. The average C_{HONO} values obtained using different normalization methods agreed well. Therefore, an estimation value of 0.47 % h^{-1} should be suitable for the nighttime conversion rate from NO_2 to HONO.

We also compared the conversion rates calculated in this study with other experiments. As shown in Table 3, $C^{\text{C}}_{\text{HONO}}$ varied widely, from 0.29 % h^{-1} to 2.40 % h^{-1}, which may be due to the various kinds of land surface in the various environments. The $C^{\text{C}}_{\text{HONO}}$ in Xiamen is comparable to those derived in Shanghai (0.70 % h^{-1} (Wang et al., 2013)), Jinan (0.68 % h^{-1} (Li et al., 2018a)), and Hong Kong (0.52 % h^{-1} (Xu et al., 2015)), less than the values calculated from most other sites, including

https://doi.org/10.5194/acp-2021-723
Preprint. Discussion started: 23 September 2021


Atmospheric Chemistry and Physics Discussions

Xinken (1.60 % h^{-1} (Su et al., 2008c)), Guangzhou (2.40 (Li et al., 2012b)), Spain (1.50 (Sörgel et al., 2011a)), Beijing (0.80 (Wang et al., 2017)), the eastern Bohai Sea (1.80 % h^{-1} (Wen et al., 2019a)), and Kathmandu (1.40 % h^{-1} (Yu et al., 2009)), but more than the value obtained in Shandong (0.29 % h^{-1} (Wang et al., 2015)). The highest C^{C}_{HONO} was found in summer, with a value of 0.55 % h^{-1}, which will be explained in Sect. 3.3.2. Another study also found that the highest C^{C}_{HONO} (1.00 % h^{-1}) appeared in summer (Wang et al., 2017).

3.3.2 The influence factors on HONO formation

The hydrolysis of NO_2 on wet surfaces producing HONO is first-order affected by the concentration of NO_2 (Finlayson-Pitts et al., 2003; Jenkin et al., 1988) and the absorption of water on the surfaces (Finlayson-Pitts et al., 2003; Kleffmann et al., 1998). A scatter plot of $HONO_{corr}/NO_2$ vs RH is shown in Fig. 6. We calculated the top-five $HONO_{corr}/NO_2$ ratios in every 5 % RH interval based on a method introduced in previous literature (Li et al., 2012b; Stutz et al., 2004), which will reduce the influence of those circumstances such as advection, the time of the night, and the surface density. These averaged maxima and standard deviations are shown in Fig. 6 as orange squares, except where data were sparse in a particular 5 % RH interval.

As for autumn and winter, the influence of RH on $HONO_{corr}/NO_2$ can be divided into two parts. The RH promoted an increase in $HONO_{corr}/NO_2$ for RH values less than 77.96 % in autumn and 91.99 % in winter, which is in line with the reaction kinetics of Reaction (R5). However, RH inhibits the conversion of NO_2 to HONO when RH is higher than a turning point. According to many previous studies, water droplets will be formed on the surface of the ground or of aerosols when RH exceeds a certain value, thus resulting in a negative dependence of $HONO_{corr}/NO_2$ on RH (He et al., 2006; Zhou et al., 2007). A similar phenomenon was also found in Guangzhou and in Shanghai (70 %, (Li et al., 2012b; Wang et al., 2013)) and in Kathmandu and in Beijing (65 %, (Yu et al., 2009; Wang et al., 2017)). However, in summer, RH appeared to promote the increase of $HONO_{corr}/NO_2$ without a turning point, suggesting that HONO production at night in summer strongly depends on RH. Another study also found a similar phenomenon in the summer in Guangzhou (Qin et al., 2009). This phenomenon might be caused by water droplets being evaporated by high temperatures. This is the reason for the highest C^{C}_{HONO} in summer. As for spring, the relationship between $HONO_{corr}/NO_2$ and RH is very complicated and needs to be explored further in the future.

It has been found that NH_3 promoted hydrolysis of NO_2 and production of HONO and NH_4NO_3(Xu et al., 2019; Li et al., 2018b). The correlations between the $HONO_{corr}/NO_2$ ratio, the NO_3^-/NO_2 ratio and the NH_3 concentration in four seasons were examined to investigate the influence of NH_3 on HONO formation through promoting hydrolysis of NO_2. Only nighttime data with RH above 80 % were chosen to avoid daytime rapid photolysis of HONO and enough water for NO_2 quick hydrolysis.(Xu et al., 2019). As shown in Fig. 7, for summer, the correlations between NH_3 and $HONO_{corr}/NO_2$ ratio was very poor and even negative (R=-0.0396), and the correlation between NO_3^-/NO_2 ratio and NH_3 was also negative (-0.2741). These results indicated that NH_3 played a minor role in HONO production in summer. For autumn, although NO_3^-/NO_2 ratio correlated well with NH_3 (R=0.3431) in autumn, $HONO_{corr}/NO_2$ ratio had bad correlation with NH_3 (R=0.0843),

https://doi.org/10.5194/acp-2021-723
Preprint. Discussion started: 23 September 2021


Atmospheric Chemistry and Physics Discussions

342 which also indicated that NH_3 played a minor role in HONO production in autumn. For spring, the correlation coefficient
343 between the $HONO_{corr}/NO_2$ ratio and the NH_3 concentration was highest among four seasons (0.3664), and the correlation
344 between the NO_3^-/NO_2 ratio and the NH_3 concentration was positive (0.1452). These phenomena proved that NH_3 might
345 promote HONO and NH_4NO_3 production through promoting NO_2 hydrolysis in spring. For winter, medium correlations were
346 found in NH_3 with both $HONO/NO_2$ ratio (R=0.2131) and NO_3^-/NO_2 ratio (R=0.2556), which indicated that NH_3 might
347 promote NO_2 hydrolysis and HONO production in winter. All in all, NH_3 might promote NO_2 hydrolysis and HONO
348 production in spring and winter, whereas NH_3 played a minor role in HONO production in summer and autumn.

349 As shown in Fig. S3, $HONO_{corr}/NO_2$ reached a pseudo-steady state from 03:00 to 06:00 LT every night. A correlation
350 analysis of $HONO_{corr}/NO_2$ with $PM_{2.5}$ was carried out in the pseudo-steady state to understand the impact of aerosols on
351 HONO production. Although we did not measure the aerosol surface density, the aerosol mass concentration can be used to
352 replace this parameter (Huang et al., 2017; Park et al., 2004; Cui et al., 2018). The positive correlation of $HONO_{corr}$ with
353 $PM_{2.5}$ (R_1 = 0.54) (Fig. 8a) may be a result of atmospheric physical processes such as convergence and diffusion. Using the
354 $HONO_{corr}/NO_2$ ratio instead of a single HONO concentration for correlation analysis with $PM_{2.5}$ reduce the impact of
355 physical processes and indicate the extent of conversion of NO_2 to HONO. Therefore, it was more credible that
356 $HONO_{corr}/NO_2$ would be moderately positively correlated with $PM_{2.5}$ (R_2 = 0.23) during the whole observation period
357 (Fig. 8b). As denoted by larger green squares in the Fig. 8b, $HONO_{corr}/NO_2$ correlated well with $PM_{2.5}$ when its
358 concentration was higher than 35 $\mu g \cdot m^{-3}$ (R_3 = 0.47). The larger the amount of HONO produced by the heterogeneous
359 reaction of NO_2 on the aerosol surface, the better the correlation between $HONO/NO_2$ and $PM_{2.5}$ (Cui et al., 2018; Wang,
360 2003; Hou et al., 2016; Li et al., 2012b; Nie et al., 2015a).

361 **3.4 Daytime sources of HONO**

362 **3.4.1 Budget analysis of HONO**

363 Having discussed the nighttime chemical behavior of HONO, we now concentrate on the daytime chemical behavior of
364 HONO. Here, $R_{unknown}$ is used to stand for the rate of emission from unknown sources. The value of $R_{unknown}$ was estimated
365 based on the balance between sources and sinks due to its short atmospheric lifetime. The sources are: (1) oxidation of NO
366 by OH ($R_{OH+NO} = k_{OH+NO}[NO][OH]$), (2) dark heterogeneous production (P_{het}), and (3) direct vehicle emission (P_{emis}); the
367 sinks are (1) HONO photolysis ($R_{phot} = J_{HONO}[HONO]$), (2) oxidation of HONO by OH ($R_{OH+HONO} =$
368 $k_{OH+HONO}[HONO][OH]$), and (3) dry deposition (L_{dep}). The value of $R_{unknown}$ can then be calculated according to

369 $$R_{unknown} = J_{HONO}[HONO] + k_{OH+HONO}[HONO][OH] + L_{dep} + \frac{\Delta[HONO]}{\Delta t} - k_{OH+NO}[NO][OH] - P_{het} - P_{emis}, \quad (5)$$

370 Where $k_{OH+HONO}$ = 6.0 × 10^{-12} cm^3 $molecules^{-1}$ s^{-1} and k_{OH+NO} = 7.4 × 10^{-12} cm^3 $molecules^{-1}$ s^{-1}, values cited from a previous
371 study(Sörgel et al., 2011b). The OH concentration ([OH]) was estimated in this study because no data for this value were
372 available. An improved empirical formula, Eq. (6), was applied to estimate [OH] using the NO_2 and HONO concentrations

https://doi.org/10.5194/acp-2021-723
Preprint. Discussion started: 23 September 2021

Atmospheric Chemistry and Physics Discussions

and the photolysis rate constants (J) of NO_2, O_3, and HONO(Wen et al., 2019b). Eq. (6) fully considers the influence of photolysis and precursors on the concentration of [OH].

$$[OH] = 4.1 \times 10^9 \times \frac{J(O^1D)^{0.83} \times J(NO_2)^{0.19} \times (140 \times NO_2 + 1) + HONO \times J(HONO)}{0.41 \times NO_2^2 + 1.7 \times NO_2 + 1 + NO \times k_{NO+OH} + HONO \times k_{HONO+OH}} \quad (6)$$

During spring, summer, autumn, and winter, the average midday OH concentrations were 8.86 × 10^6 cm^{-3}, 1.48 × 10^7 cm^{-3}, 1.36 × 10^7 cm^{-3}, and 6.19 × 10^6 cm^{-3}, respectively, which were within the range of those obtained in other studies varying from 4 × 10^6 cm^{-3} to 1.7 × 10^7 cm^{-3} (Tan et al., 2017; Lu et al., 2013).

$\frac{\Delta[HONO]}{\Delta t}$ is the observed change of HONO concentration(ppb·s^{-1}). The value of $\frac{\Delta[HONO]}{\Delta t}$ is the concentration difference between the center of one interval (1 min) and the center of the next interval, and this accounts for changes in concentration levels (Sörgel et al., 2011a). The parameter L_{dep} can be quantified by multiplying the dry deposition rate of HONO by the observed HONO concentration and then dividing by the mixing layer height ($L_{dep} = \frac{v_{HONO}^{ground} \times [HONO]}{H}$). A value of v_{HONO}^{ground} = 2 cm·s^{-1} was used for the deposition rate (Sörgel et al., 2011a; Su et al., 2008b). The mixing layer heights during spring, summer, autumn, and winter were 1074.4 m, 1173.8 m, 1494.6 m, and 1310.4 m, respectively (Gao, 1999). In summarizing the known HONO sources, we included the nighttime heterogeneous production as a known source based on the assumption that the day continues in the same way as the night (Sörgel et al., 2011a). The term P_{het} was parameterized by NO_2 conversion at night using the formula $P_{het} = C_{HONO}^{C}[NO_2]$ (Alicke, 2002).

Figure 9 shows the contributions of each term in Eq. (7) to the HONO budgets in different seasons. Photolysis of HONO (R_{phot}) formed the largest proportion of the sinks in all four seasons, accounting for 95.33 %, 94.60 %, 95.46 %, and 96.18 % in spring, summer, autumn, and winter, respectively. The value of R_{phot} in summer was the highest (3.65 ppb·h^{-1}), followed by spring (3.17 ppb·h^{-1}), winter (2.48 ppb·h^{-1}) and autumn (2.42 ppb·h^{-1}). The oxidation of HONO by OH contributed little to HONO sinks (2.97 % of all sinks). Dry deposition (L_{dep}) was also very small (1.63 % of all sinks). As for known sources, R_{OH+NO} was the main known source in all four seasons, wherein the largest proportion was found in summer (63.24 %), followed by autumn (52.36 %), spring (52.02 %), and winter (49.99 %). Direct emission was second among the known sources, accounting for 39.58 %, 29.15 %, 38.36 %, and 43.03 % in spring, summer, autumn, and winter, respectively. Dark heterogeneous formation (P_{het}) was almost negligible in the daytime, accounting for approximately 8.07 % of known sources during the whole observation period. As for unknown sources, these made up the largest proportion of all sources found in summer (79.55 %), followed by autumn (71.51 %), spring (69.67 %) and winter (55.63 %).

It is worth noting that $R_{unknown}$ exhibited a maximum around noon in all seasons. A previous study in Wangdu (Liu et al., 2019d) also found that unknown sources of HONO reached a maximum at midday, with the strongest photolysis rates in summer. This strengthens the validity of the assumption that the missing HONO formation mechanism is related to a photolytic source (Michoud et al., 2014). In the present study, the daily maximum $R_{unknown}$ value was 4.35 ppb·h^{-1} in summer,

https://doi.org/10.5194/acp-2021-723
Preprint. Discussion started: 23 September 2021

Atmospheric Chemistry and Physics Discussions

403 followed by 3.53 ppb·h^{-1} in spring, 3.13 ppb·h^{-1} in autumn and 2.05 ppb·h^{-1} in winter. Average $R_{unknown}$ during the whole
404 observation was 2.16 ppb·h^{-1}, which was almost at the upper-middle level of studies reported: 0.5 ppb·h^{-1} in a forest near
405 Jülich, Germany(Kleffmann, 2005); 0.77 ppb·h^{-1} at a rural site in the Pearl River delta, China (Li et al., 2012a); 1.04 ppb·h^{-1}
406 at a suburban site in Nanjing, China(Liu et al., 2019a); ≈2 ppb·h^{-1} in Xinken, China(Su et al., 2008a); and 2.95 ppb·h^{-1} in the
407 urban atmosphere of Jinan, China(Li et al., 2018a).

408 **3.4.2 Exploration of possible unknown daytime sources**

409 According to the analyses in Sect. 3.1 and Sect. 3.4.1, the unknown sources are likely to be related to light. It was indeed
410 found that the unknown sources have a good correlation with the parameters related to light. It was reported in previous
411 studies that particulate nitrate photolysis is a source of HONO (Ye et al., 2017; Ye et al., 2016; Scharko et al., 2014; Romer
412 et al., 2018; Mcfall et al., 2018). We will discuss the possibility of HONO being produced by photolysis of particulate nitrate
413 ($J(NO_3\_R) \times pNO_3^-$) at this site in the next section. There was a logarithmic relationship showing good correlation between
414 $R_{unknown}$ (ppb·h^{-1}) and $J(NO_3^-\_R) \times pNO_3^-$ (μg·m^{-3}·s^{-1}) in spring (R^2 = 0.5982) and summer (R^2 = 0.5837), while relatively
415 weak correlation was found in autumn (R^2 = 0.2131) and winter (R^2 = 0.3764) (Fig. 10). This result indicated that photolysis
416 of particulate nitrate contributed more in spring and summer than in autumn and winter. In conditions of relatively lower
417 $J(NO_3\_R) \times pNO_3^-$, $R_{unknown}$ increased rapidly with increasing pNO_3^- concentration and its photolysis rate constant but
418 reached a plateau after a critical value ($J(NO_3\_R) \times pNO_3^- > 0.5$ μg·m^{-3}·s^{-1} in summer and autumn, and $J(NO_3\_R) \times$
419 $pNO_3^- > 1.5$ μg·m^{-3}·s^{-1} in winter). There was no obvious turning point in spring, but it could be seen that the growth rate
420 was declining. This indicated that in conditions that were relatively cleaner, the missing daytime source of HONO was
421 limited by the pNO_3^- concentration and the photolysis rate constant. However, with enough particulate nitrate providing
422 sufficient precursor or enough light to stimulate the reaction, the HONO production did not increase as $J(NO_3\_R) \times pNO_3^-$
423 increased. Other generation mechanisms might play leading roles in the condition with enough particulate nitrate or enough
424 light. It was found in a previous study that heterogeneous soot photochemistry may contribute to the daytime HONO
425 concentration(Monge et al., 2010). Black carbon (BC) values were as a substitute for soot values(Sörgel et al., 2011b). When
426 BC concentration was above 2.0 μg·m^{-3}, the missing daytime source of HONO did not increase as $J(NO_3\_R) \times pNO_3^-$
427 increased. We found that the missing daytime source of HONO correlated better with BC×UV (R=0.9247, R=0.6421) than
428 with BC (R=0.5012, R=0.5720) or UV (R=0.8556, R=0.4230) alone in autumn and winter (Fig. S4), probably related to the
429 conversion of NO_2 to HONO on BC enhanced by light.

430 We discuss whether photolysis of particulate nitrate was able to provide enough additional HONO by estimating the rate of
431 HONO production by nitrate photolysis in spring and summer (Zhou et al., 2007; Li et al., 2012b; Wang et al., 2017) using

432 $$J_{NO_3^-\rightarrow HONO} = \frac{R_{unknown} \times H}{f \times [NO_3^-] \times \upsilon_{NO_3^-} \times t_d}, \quad (7)$$

https://doi.org/10.5194/acp-2021-723
Preprint. Discussion started: 23 September 2021

Atmospheric Chemistry and Physics Discussions

where $J_{NO_3^- \rightarrow HONO}$ is the rate of photolysis of NO_3^- to form HONO, $\upsilon_{NO_3^-}$ is the dry deposition rate of NO_3^- during the period t_d, and f is the proportion of the surface exposed to the sun at midday. Here, we suppose that the surfaces involving NO_3^- were exposed to light by a factor $f = 1/4$, taking mixing height $H = 250\ m$, $\upsilon_{NO_3^-}$ = 5 cm·s^{-1} over t_d = 24 h. We use the mean midday value of $R_{unknown}$ = 9.77 μg·m^{-3}·h^{-1} and [NO_3^-] = 10.52 μg·m^{-3} in spring; and $R_{unknown}$ = 12.04μg·m^{-3}·h^{-1} and [NO_3^-] = 3.59 μg·m^{-3} in summer. The photolysis rates $J_{NO_3^- \rightarrow HONO}$ derived from Eq. (8) were 5.97 × 10^{-5} s^{-1} and 1.99 × 10^{-4} s^{-1} for spring and summer, respectively. These values were in the range 6.2 × 10^{-6} to 5.0 × 10^{-4} obtained in a previous study (Ye et al., 2017), which indicated that particulate nitrate photolysis could be likely source for the missing daytime additional HONO formation in spring and summer. The variability of $J_{NO_3^- \rightarrow HONO}$ may be caused by chemical composition, acidity, light-absorbing constituents, and the optical and other physical properties of aerosols.

3.5 Parameterization of HONO

Through an empirical parameterized formula, we can explore an accurate parameterization method for HONO, discuss the main control factors for the HONO concentration and its chemical behavior, and quantify its main sources and key kinetic parameters. As mentioned in Sect. 3.1, the HONO/NO_x ratio is better than HONO/NO_2 as an indicator of HONO generation. In another study (Elshorbany et al., 2012), data were collected from 15 field observations all over the world to establish the correlation between the HONO/NO_x ratio and the HONO concentration in global models. Therefore, we applied this method in this study to parameterize the HONO concentration. As shown in Fig. 11, the HONO/NO_x ratios in the four seasons were close to the calculated value (0.02). However, there were seasonal variations in the slope, showing a maximum in summer (2.60 × 10^{-2}), followed by autumn (2.06 × 10^{-2}), and a minimum in winter (1.59 × 10^{-2}). Except for in spring, HONO showed good correlation with NO_x, with R^2 values ranging from 0.8972 to 0.9621. Therefore, we used slopes of 2.60 × 10^{-2}, 2.06 × 10^{-2}, and 1.59 × 10^{-2} to parameterize the HONO concentrations in summer, autumn, and winter, respectively. As for spring, though only a weak correlation between HONO and NO_x was found, the majority of the HONO/NO_x ratios fluctuated round a slope of 0.02 because concentrations of NO_x greater than 60 ppb only accounted for 8.83 % of the data. Therefore, a slope of 0.02 was applied in spring to parameterize the HONO concentration.

As can be seen from Fig. 12, the estimated values are very close to the observed values in the nighttime in autumn. After sunrise and before noon, the values observed were higher than the estimated values, and this difference gradually increases. After noon and before sunset, the values observed were still higher than the values estimated, but the difference gradually decreases. This phenomenon was also found in the daytime in spring and summer, but not in winter. Compared with the daytime, the estimated values during the nighttime were closer to the observed values in both trend and value in all four seasons, which further demonstrates that nighttime HONO is mainly produced from the direct vehicle emissions and heterogeneous reaction of NO_2 on the ground or the surfaces of aerosols. Therefore, we should pay much more attention to simulation in the daytime. We distinguish two main sectors, nighttime and daytime, to analyze the factors affecting the

https://doi.org/10.5194/acp-2021-723
Preprint. Discussion started: 23 September 2021


Atmospheric Chemistry and Physics Discussions

HONO diurnal variation (Liu, 2017). Although J(HONO)×HONO also correlated well with $J(NO_2)\times NO_2$ in all four seasons in this study and the linear fitting coefficients fluctuated around 0.01 in all four seasons (Fig. S5), bad simulation results during the daytime were found (Fig. S6) using

$$[HONO] = k \times [NO_2] \times J(NO_2)/J(HONO). \quad (8)$$

Where k was the linear fitting coefficient between J(HONO)×HONO and $J(NO_2)\times NO_2$. In contrast, excellent simulation results were found in a previous study using the same formula (Liu, 2017), which suggests that using the same simulation formula in different regions may obtain greatly varying results. Eq. (8) can be regarded as a combination of $[NO_2]$ with $J(NO_2)/J$(HONO). $J(NO_2)/J$(HONO) kept relatively constant (5.48~5.87) in the daytime in four seasons. Therefore, diurnal variation of [HONO] simulated by Eq. (8) depended on $[NO_2]$ (Fig. S7). Eq. (8) is only suitable for regions where the diurnal variation of $[NO_2]$ is consistent with that of [HONO].

As discussed in Sect. 3.4.2, nitrate photolysis was perhaps the source of HONO in this study. Besides, the difference between the observed value and the simulated value kept increasing before noon and the difference began to decrease after noon, which was consistent with nitrate photolysis. Therefore, we take the photolysis of nitrate into the HONO concentration simulation. The specific formulas for the simulation of spring, summer, autumn and winter as shown as follow:

$$HONOspring = 2.00 \times 10^{-2} \times NOx + [NO_3^-] \times J(NO_3\_R)/4 \quad (9)$$

$$HONOsummer = 2.60 \times 10^{-2} \times NOx + [NO_3^-] \times J(NO_3\_R) \quad (10)$$

$$HONOautumn = 2.06 \times 10^{-2} \times NOx + [NO_3^-] \times J(NO_3\_R) \quad (11)$$

$$HONOwinter = 1.59 \times 10^{-2} \times NOx + [NO_3^-] \times J(NO_3\_R)/4 \quad (12)$$

In this way, the daytime simulation results are significantly improved (Fig. 12). This further demonstrates that the apportionment of HONO sources is credible. The parameterization described in this work was more reasonable and can be better used in the future in such coastal sites.

3.6 Comparison of contributions of HONO and O_3 to OH radicals

Comparing the OH radical production via photolysis of HONO and O_3, the effect of the high HONO concentrations in the daytime on the tropospheric oxidation capacity was evaluated (Ryan et al., 2018). Nitrous acid is considered to be a crucial source of OH radicals (Lee et al., 2016). As shown in Eq. (12), OH production rates from O_3 photolysis ($P_{OH}(O_3)$) were calculated based on $[O_3]$, $J(O^1D)$, and $[H_2O]$ (Liu et al., 2019c). Only $O(^1D)$ atoms produced by the O_3 photolysis at UV wavelengths less than 320 nm (R6) can combine with water to generate OH radicals (R7) in the atmosphere. The absolute water concentration was derived from temperature and RH. The reaction (R8) rates for N_2 is 3.1×10^{-11} cm^3 molecules^{-1} s^{-1} and for O_2 is 4.0×10^{-11} cm^3 molecules^{-1} s^{-1}(Liu et al., 2019a). The net OH formation from HONO was estimated by Eq. (13)

https://doi.org/10.5194/acp-2021-723
Preprint. Discussion started: 23 September 2021


Atmospheric Chemistry and Physics Discussions

(Su et al., 2008b; Sörgel et al., 2011a; Li et al., 2018a; Atkinson et al., 2004). In addition to the two primary production of OH radicals mentioned above, there are the reaction of organic and hydro peroxy radicals (RO_2 and HO_2) with NO, hydrogen peroxide photolysis and the ozonolysis of alkenes (Hofzumahaus et al., 2009; Gligorovski et al., 2015; Wang et al., 2018).

$$P_{OH}(O_3) = 2J(O^1D)[O_3]\phi OH,\ \ \phi OH = k_7[H_2O]/(k_7[H_2O] + k_8[M]) \quad (12)$$

$$O_3 + h\nu \rightarrow O(\,^1D) + O_2\ (h\nu < 320\ \text{nm}) \quad (R6)$$

$$O(\,^1D) + H_2O \rightarrow 2OH \quad (R7)$$

$$O(\,^1D) + M \rightarrow O(\,^3P) + M\ (M \text{ is } N_2 \text{ or } O_2) \quad (R8)$$

$$P_{OH}(HONO) = J_{HONO}[HONO] - k_{OH+NO}[NO][OH] - k_{OH+HONO}[HONO][OH] \quad (13)$$

The diurnal patterns of P(OH) are shown in Fig. 13. The formation rates of OH from O_3 photolysis peaked in midday at around 0.71 ppb·h^{-1}, 5.80 ppb·h^{-1}, 2.21 ppb·h^{-1}, and 0.48 ppb·h^{-1} for spring, summer, autumn, and winter, respectively. The variation of $P_{OH}(O_3)$ is consistent with $J(O^1D)$ (Fig. S8), peaking in midday and in summer on a diurnal and a seasonal timescale, respectively. For summer and autumn, P_{OH}(HONO) had a similar trend as $P_{OH}(O_3)$, peaking at around noon at the time of the highest J(HONO), but this was negligible at sunrise and sunset (Fig. S9). For spring and winter, however, P_{OH}(HONO) reached a maximum in the morning rush hour caused by the combined influences of high HONO concentration and high J(HONO). A similar result was also found in southwest Spain from mid-November to mid-December 2008 (Sörgel et al., 2011a).The HONO photolysis contributed significantly more OH than O_3 photolysis during the whole daytime in spring, autumn, and winter. In summer, the HONO photolysis contributed to more OH in the early morning, and although the O_3 photolysis produced more in the afternoon, HONO photolysis had a considerable effect on OH production. A similar result was also found in Nanjing of eastern China from November 2017 to November 2018(Liu et al., 2019a). These results show that HONO contributes considerably to the atmospheric oxidizing capacity of the suburban atmosphere of Xiamen. Although HONO concentrations (average: 0.66 ppb) are much lower than O_3 concentrations (average: 35.88 ppb) during 07:00–16:00 LT, daytime HONO photolysis forms significantly more OH than daytime photolysis of O_3 in four seasons except for summer afternoon. Generally, the mean value of P_{OH}(HONO) from 07:00 to 16:00 LT was 1.89 ppb·h^{-1}, and the average $P_{OH}(O_3)$ was 1.14 ppb·h^{-1}. A similar result was found in Melbourne, where the peak OH production rate reached 2 ppb·h^{-1} from 0.4 ppb HONO (Ryan et al., 2018). The important role of HONO in the production of OH promotes photochemical peroxyacetyl nitrate formation (Hu et al., 2020).

4. Conclusions

We conducted measurements of HONO in the atmosphere at an IUE supersite in a coastal city of southeastern China in August, October, and December 2018 and March 2019, finding an average HONO concentration of 0.54 ± 0.47 ppb across

https://doi.org/10.5194/acp-2021-723
Preprint. Discussion started: 23 September 2021


Atmospheric Chemistry and Physics Discussions

the whole observation period. Concentrations of HONO in spring and summer were higher than in winter and autumn, which was consistent with seasonal variations in RH. Both higher HONO concentrations in the daytime and the HONO/NO_x ratio peaking around noon suggested that additional sources of HONO might be related to light. It was found that the contribution from vehicle exhaust emissions (1.64 %) was higher than that found in most other studies due to the site being surrounded by several expressways with a large number of passing diesel vehicles. The average nocturnal conversion rate of NO_2 to HONO was 0.47 % h^{-1}, which was within the range 0.29–2.40 % h^{-1} found by other studies. The $HONO_{corr}/NO_2$ ratio increased with RH and the concentration of $PM_{2.5}$ during the nighttime, which indicates that nocturnal heterogeneous reactions on the surfaces of aerosols are the major source of HONO. However, dark heterogeneous formation (P_{hete}) was almost negligible in the daytime, accounting for approximately 8.07 % of known sources across the whole observation period. $R_{unknown}$ made up at the largest proportion of all sources in summer (79.55 %), autumn (71.51 %), spring (69.67 %), and winter (55.64 %). It was found that there was a logarithmic relationship between $R_{unknown}$ and particulate nitrate photolysis in four seasons. The variation of HONO at night can be accurately simulated based on the HONO/NO_x ratio, while $J(NO_3^-\_R) \times pNO_3^-$ or $1/4 \times (J(NO_3^-\_R) \times pNO_3^-)$ should be considered for daytime simulation. Local tropospheric oxidation capacity was significantly increased by HONO during 07:00–16:00, providing an OH radical source 1.89 ppb·h^{-1}.

Data availability

The observation data at this site are available from the authors upon request.

Authorship Contribution Statement

Baoye Hu and Jun Duan contributed equally to this work. Baoye Hu and Jun Duan collected the HONO data and analyzed the data. Baoye Hu wrote the manuscript. Baoye Hu, Jun Duan performed the experiments. Jun Duan and Fang Wu built equipment of IBBCEEAS. Youwei Hong, Min Qin and Jinsheng Chen revised manuscript. Min Qin, Pinhua Xie and Jinsheng Chen designed the manuscript. Jinsheng Chen supported funding of observation and research. Lingling Xu, Mengren Li, Yahui Bian contributed to discussions of results.

Competing interests

The authors declare that they have no conflict of interest.

Acknowledgments

This study was funded by the Cultivating Project of Strategic Priority Research Program of Chinese Academy of Sciences (XDPB1903), the National Key Research and Development Program (2017YFC0209400, 2016YFC02005,

https://doi.org/10.5194/acp-2021-723
Preprint. Discussion started: 23 September 2021


Atmospheric Chemistry and Physics Discussions

549 2016YFC0112200), the National Natural Science Foundation of China (41575146, 41875154), the FJIRSM&IUE Joint
550 Research Fund (RHZX-2019-006), the Center for Excellence in Regional Atmospheric Environment, CAS (E0L1B20201),
551 State Key Laboratory of Environmental Chemistry and Ecotoxicology, Research Center for Eco-Environmental Sciences,
552 CAS and Xiamen Atmospheric Environment Observation and Research Station of Fujian Province.

553 **Supplementary information**

554 Attached please find supplementary information associated with this article.

https://doi.org/10.5194/acp-2021-723
Preprint. Discussion started: 23 September 2021

Atmospheric Chemistry and Physics Discussions

555

556 **References**

557 Acker, K., Febo, A., Trick, S., Perrino, C., Bruno, P., Wiesen, P., Möller, D., Wieprecht, W., Auel, R., Giusto, M., Geyer, A., Platt, U., and
558 Allegrini, I.: Nitrous acid in the urban area of Rome, Atmos. Environ., 40, 3123-3133, 10.1016/j.atmosenv.2006.01.028, 2006.

559 Alicke, B.: Impact of nitrous acid photolysis on the total hydroxyl radical budget during the Limitation of Oxidant Production/Pianura
560 Padana Produzione di Ozono study in Milan, J. Geophys. Res., 107, 10.1029/2000jd000075, 2002.

561 Ammann, M., Kalberer, M., Jost, D. T., Tobler, L., Ro¨ssler, E., Piguet, D., Ga¨ggeler, H. W., and Baltensperger, U.: Heterogeneous
562 production of nitrous acid on soot in polluted air masses, Nature, 395, 157-160, 1998.

563 Atkinson, R., Baulch, D. L., Cox, R. A., Crowley, J. N., Hampson, R. F., Hynes, R. G., Jenkin, M. E., Rossi, M. J., and Troe, J.: Evaluated
564 kinetic and photochemical data for atmospheric chemistry: Volume I – gas phase reactions of O*x*, HO*x*, NO*x* and SO*x* species, Atmos.
565 Chem. Phys., 4, 1461–1738, 2004.

566 Aubin, D. G. and Abbatt, J. P.: Interaction of NO_2 with hydrocarbon soot: Focus on HONO yield, surface modification, and mechanism, J.
567 Phys. Chem. A 111, 6263-6273, 2007.

568 Chang, Y., Zou, Z., Deng, C., Huang, K., Collett, J. L., Lin, J., and Zhuang, G.: The importance of vehicle emissions as a source of
569 atmospheric ammonia in the megacity of Shanghai, Atmos. Chem. Phys., 16, 3577-3594, 10.5194/acp-16-3577-2016, 2016.

570 Cui, L., Li, R., Zhang, Y., Meng, Y., Fu, H., and Chen, J.: An observational study of nitrous acid (HONO) in Shanghai, China: The aerosol
571 impact on HONO formation during the haze episodes, Sci. Total. Environ., 630, 1057-1070, 10.1016/j.scitotenv.2018.02.063, 2018.

572 Duan, J., Qin, M., Ouyang, B., Fang, W., Li, X., Lu, K., Tang, K., Liang, S., Meng, F., Hu, Z., Xie, P., Liu, W., and Häsler, R.:
573 Development of an incoherent broadband cavity-enhanced absorption spectrometer for in situ measurements of HONO and NO_2, Atmos.
574 Meas. Tech., 11, 4531–4543, 10.5194/amt-11-4531-2018, 2018.

575 Elshorbany, Y. F., Steil, B., Brühl, C., and Lelieveld, J.: Impact of HONO on global atmospheric chemistry calculated with an empirical
576 parameterization in the EMAC model, Atmos. Chem. Phys., 12, 9977-10000, 10.5194/acp-12-9977-2012, 2012.

577 Elshorbany, Y. F., Kurtenbach, R., Wiesen, P., Lissi, E., Rubio, M., Villena, G., Gramsch, E., Rickard, A. R., Pilling, M. J., and
578 Kleffmann, J.: Oxidation capacity of the city air of Santiago, Chile, Atmos. Chem. Phys., 9, 2257–2273, https://www.atmos-chem-
579 phys.net/9/2257/2009/, 2009.

580 Finlayson-Pitts, B. J., Wingen, L. M., Sumner, A. L., Syomin, D., and Ramazan, K. A.: The heterogeneous hydrolysis of NO2 in
581 laboratory systems and in outdoor and indoor atmospheres: An integrated mechanism, Phys. Chem. Chem. Phys., 5, 223-242,
582 10.1039/b208564j, 2003.

583 Fu, X., Wang, T., Zhang, L., Li, Q., Wang, Z., Xia, M., Yun, H., Wang, W., Yu, C., Yue, D., Zhou, Y., Zheng, J., and Han, R.: The
584 significant contribution of HONO to secondary pollutants during a severe winter pollution event in southern China, Atmos. Chem. Phys.,
585 19, 1-14, 10.5194/acp-19-1-2019, 2019.

586 Gao, J.: An analysis of some pollution weather conditions, Journal of Oceanography in Taiwan Strait, 18, 55-62, 1999.

587 Ge, S., Wang, G., Zhang, S., Li, D., Xie, Y., Wu, C., Yuan, Q., Chen, J., and Zhang, H.: Abundant NH3 in China Enhances Atmospheric
588 HONO Production by Promoting the Heterogeneous Reaction of SO2 with NO2, Environ Sci Technol, 53, 14339-14347,
589 10.1021/acs.est.9b04196, 2019.

590 George, C., Strekowski, R. S., Kleffmann, J., Stemmler, K., and Ammann, M.: Photoenhanced uptake of gaseous NO2 on solid organic
591 compounds: a photochemical source of HONO?, Faraday Discuss, 130, 195-210; discussion 241-164, 519-124, 10.1039/b417888m, 2005.

592 Gil, J., Kim, J., Lee, M., Lee, G., Lee, D., Jung, J., An, J., Hong, J., Cho, S., Lee, J., and Long, R.: The role of HONO in O3 formation and
593 insight into its formation mechanism during the KORUS-AQ Campaign, Atmos. Chem. Phys. Discuss, 10.5194/acp-2019-1012, 2019.

594 Gligorovski, S., Strekowski, R., Barbati, S., and Vione, D.: Environmental Implications of Hydroxyl Radicals ((*)OH), Chem Rev, 115,
595 13051-13092, 10.1021/cr500310b, 2015.

596 Gutzwiller, L., Arens, F., Baltensperger, U., Ga¨ggeler, H. W., and Ammann, M.: Significance of Semivolatile Diesel Exhaust Organics
597 for Secondary HONO Formation, Environ. Sci. Technol. , 36, 677-682, 2002.

598 He, Y., Zhou, X., Hou, J., Gao, H., and Bertman, S. B.: Importance of dew in controlling the air-surface exchange of HONO in rural
599 forested environments, Geophys. Res. Lett., 33, 10.1029/2005gl024348, 2006.

600 Hofzumahaus, A., Rohrer, F., Lu, K., Bohn, B., Brauers, T., Chang, C.-C., Fuchs, H., Holland, F., Kita, K., Kondo, Y., Li, X., Lou, S.,
601 Shao, M., Zeng, L., Wahner, A., and Zhang, Y.: Amplified Trace Gas Removal in the Troposphere, Science, 324, 1702-1704, 2009.

602 Hou, S., Tong, S., Ge, M., and An, J.: Comparison of atmospheric nitrous acid during severe haze and clean periods in Beijing, China,
603 Atmos. Environ. , 124, 199-206, 10.1016/j.atmosenv.2015.06.023, 2016.

604 Hu, B., Liu, T., Hong, Y., Xu, L., Li, M., Wu, X., Wang, H., Chen, J., and Chen, J.: Characteristics of peroxyacetyl nitrate (PAN) in a
605 coastal city of southeastern China: Photochemical mechanism and pollution process, Sci. Total Environ., 719, 137493,
606 10.1016/j.scitotenv.2020.137493, 2020.

607 Huang, R. J., Yang, L., Cao, J., Wang, Q., Tie, X., Ho, K. F., Shen, Z., Zhang, R., Li, G., Zhu, C., Zhang, N., Dai, W., Zhou, J., Liu, S.,
608 Chen, Y., Chen, J., and O'Dowd, C. D.: Concentration and sources of atmospheric nitrous acid (HONO) at an urban site in Western China,
609 Sci. Total Environ., 593-594, 165-172, 10.1016/j.scitotenv.2017.02.166, 2017.

610 Jenkin, M. E., Cox, R. A., and Williams, D. J.: Laboratory studies of the kinetics of formation of nitrous acid from the thermal reaction of
611 nitrogen dioxide and water vapour, Atmos. Environ., 22, 487-498, 1988.

612 Kasibhatla, P., Sherwen, T., Evans, M. J., Carpenter, L. J., Reed, C., Alexander, B., Chen, Q., Sulprizio, M. P., Lee, J. D., Read, K. A.,
613 Bloss, W., Crilley, L. R., Keene, W. C., Pszenny, A. A. P., and Hodzic, A.: Global impact of nitrate photolysis in sea-salt aerosol on NOx,
614 OH, and O3 in the marine boundary layer, Atmos. Chem. Phys., 18, 11185-11203, 10.5194/acp-18-11185-2018, 2018.

615 Kirchner, U., Scheer, V., and Vogt, R.: FTIR Spectroscopic Investigation of the Mechanism and Kinetics of the Heterogeneous Reactions
616 of NO2 and HNO3 with Soot, J. Phys. Chem. A, 104, 8908-8915, 2000.

617 Kirchstetter, T. W., Harley, R. A., and Littlejohn, D.: Measurement of Nitrous Acid in Motor Vehicle Exhaust, Environ. Sci. Technol., 30,
618 2843-2849, 1996.

619 Kleffmann, J.: Daytime formation of nitrous acid: A major source of OH radicals in a forest, Geophys. Res. Lett., 32,
620 10.1029/2005gl022524, 2005.

621 Kleffmann, J.: Daytime sources of nitrous acid (HONO) in the atmospheric boundary layer, Chem. phys. chem, 8, 1137-1144,
622 10.1002/cphc.200700016, 2007.

623 Kleffmann, J., Becker, K., and Wiesen, P.: Heterogeneous NO_2 conversion processes on acid surfaces: Possible atmospheric implications,
624 Atmos. Environ., 32, 2721–2729, https://doi.org/10.1016/S1352-2310(98)00065-X, 1998.

625 Kramer, L. J., Crilley, L. R., Adams, T. J., Ball, S. M., Pope, F. D., and Bloss, W. J.: Nitrous acid (HONO) emissions under real-world
626 driving conditions from vehicles in a UK road tunnel, Atmos. Chem. Phys., 20, 5231-5248, 10.5194/acp-20-5231-2020, 2020.

627 Kurtenbacha, R., Beckera, K. H., Gomesa, J. A. G., Kleffmanna, J., L.orzera, J. C., Spittlera, M., Wiesena, P., Ackermannb, R., Geyerb, A.,
628 and Plattb, U.: Investigations of emissions and heterogeneous formation of HONO in a road traffic tunnel, Atmos. Environ., 35, 3385-3394,
629 2001.

630 Lee, B. H., Wood, E. C., Herndon, S. C., Lefer, B. L., Luke, W. T., Brune, W. H., Nelson, D. D., Zahniser, M. S., and Munger, J. W.:
631 Urban measurements of atmospheric nitrous acid: A caveat on the interpretation of the HONO photostationary state, J. Geophys. Res.
632 Atmos., 118, 12,274-212,281, 10.1002/2013jd020341, 2013.

633 Lee, J. D., Whalley, L. K., Heard, D. E., Stone, D., Dunmore, R. E., Hamilton, J. F., Young, D. E., Allan, J. D., Laufs, S., and Kleffmann,
634 J.: Detailed budget analysis of HONO in central London reveals a missing daytime source, Atmos. Chem. Phys., 16, 2747-2764,
635 10.5194/acp-16-2747-2016, 2016.

636 Lei, L., Zhiyao, D., Hui Li, Chongqin Zhu, Graeme Henkelman, Joseph S. Franciscoa, and Zeng, X. C.: Formation of HONO from the
637 NH3-promoted hydrolysis of NO_2 dimers in the atmosphere, Proc. Natl. Acad. Sci. USA, 115, 7236–7241,
638 https://doi.org/10.1073/pnas.1807719115 2018.

639 Li, D., Xue, L., Wen, L., Wang, X., Chen, T., Mellouki, A., Chen, J., and Wang, W.: Characteristics and sources of nitrous acid in an
640 urban atmosphere of northern China: Results from 1-yr continuous observations, Atmos. Environ., 182, 296-306,
641 10.1016/j.atmosenv.2018.03.033, 2018a.

https://doi.org/10.5194/acp-2021-723
Preprint. Discussion started: 23 September 2021

Atmospheric Chemistry and Physics Discussions

Li, G., Lei, W., Zavala, M., Volkamer, R., Dusanter, S., Stevens, P., and Molina, L. T.: Impacts of HONO sources on the photochemistry in Mexico City during the MCMA-2006/MILAGO Campaign, Atmos. Chem. Phys., 10, 6551-6567, 10.5194/acp-10-6551-2010, 2010.

Li, L., Duan, Z., Li, H., Zhu, C., Henkelman, G., Francisco, J. S., and Zeng, X. C.: Formation of HONO from the NH3-promoted hydrolysis of NO2 dimers in the atmosphere, Proc Natl Acad Sci U S A, 115, 7236-7241, 10.1073/pnas.1807719115, 2018b.

Li, S., Matthews, J., and Sinha, A.: Atmospheric Hydroxyl Radical Production from Electronically Excited NO_2 and H_2O, Science, 319, 2008.

Li, X., Brauers, T., Häseler, R., Bohn, B., Fuchs, H., Hofzumahaus, A., Holland, F., Lou, S., Lu, K. D., Rohrer, F., Hu, M., Zeng, L. M., Zhang, Y. H., Garland, R. M., Su, H., Nowak, A., Wiedensohler, A., Takegawa, N., Shao, M., and Wahner, A.: Exploring the atmospheric chemistry of nitrous acid (HONO) at a rural site in Southern China, Atmos. Chem. Phys., 12, 1497-1513, 10.5194/acp-12-1497-2012, 2012a.

Li, X., Brauers, T., Häseler, R., Bohn, B., Fuchs, H., Hofzumahaus, A., Holland, F., Lou, S., Lu, K. D., Rohrer, F., Hu, M., Zeng, L. M., Zhang, Y. H., Garland, R. M., Su, H., Nowak, A., Wiedensohler, A., Takegawa, N., Shao, M., and Wahner, A.: Exploring the atmospheric chemistry of nitrous acid (HONO) at a rural site in Southern China, Atmos. Chem. Phys., 12, 1497-1513, 10.5194/acp-12-1497-2012, 2012b.

Li, X., Rohrer, F., Hofzumahaus, A., Brauers, T., Häseler, R., Bohn, B., Broch, S., Fuchs, H., Gomm, S., Holland, F., Jäger, J., Kaiser, J., Keutsch, F. N., Lohse, I., Lu, K., Tillmann, R., Wegener, R., Wolfe, G. M., Mentel, T. F., Kiendler-Scharr, A., and Wahner, A.: Missing Gas-Phase Source of HONO Inferred from Zeppelin Measurements in the Troposphere, Science, 344, 2014.

Liu, T., Hu, B., Yang, Y., Li, M., Hong, Y., Xu, X., Xu, L., Chen, N., Chen, Y., Xiao, H., and Chen, J.: Characteristics and source apportionment of PM2.5 on an island in Southeast China: Impact of sea-salt and monsoon, Atmos. Res., 235, 104786, 10.1016/j.atmosres.2019.104786, 2020.

Liu, Y.: Observations and parameterized modelling of ambient nitrous acid (HONO) in the megacity areas of the eastern China Peking University, China, 161 pp., 2017.

Liu, Y., Nie, W., Xu, Z., Wang, T., Wang, R., Li, Y., Wang, L., Chi, X., and Ding, A.: Semi-quantitative understanding of source contribution to nitrous acid (HONO) based on 1 year of continuous observation at the SORPES station in eastern China, Atmos. Chem. Phys., 19, 13289-13308, 10.5194/acp-19-13289-2019, 2019a.

Liu, Y., Nie, W., Xu, Z., Wang, T., Wang, R., Li, Y., Wang, L., Chi, X., and Ding, A.: Contributions of different sources to nitrous acid (HONO) at the SORPES station in eastern China: results from one-year continuous observation, Atmos. Chem. Phys. Discuss., 1-47, 10.5194/acp-2019-219, 2019b.

Liu, Y., Nie, W., Xu, Z., Wang, T., Wang, R., Li, Y., Wang, L., Chi, X., and Ding, A.: Semi-quantitative understanding of source contribution to nitrous acid (HONO) based on 1 year of continuous observation at the SORPES station in eastern China, Atmos. Chem. Phys., 19, 13289-13308, 10.5194/acp-19-13289-2019, 2019c.

Liu, Y., Lu, K., Li, X., Dong, H., Tan, Z., Wang, H., Zou, Q., Wu, Y., Zeng, L., Hu, M., Min, K. E., Kecorius, S., Wiedensohler, A., and Zhang, Y.: A Comprehensive Model Test of the HONO Sources Constrained to Field Measurements at Rural North China Plain, Environ. Sci. Technol., 10.1021/acs.est.8b06367, 2019d.

Liu, Z., Wang, Y., Costabile, F., Amoroso, A., Zhao, C., Huey, L. G., Stickel, R., Liao, J., and Zhu, T.: Evidence of aerosols as a media for rapid daytime HONO production over China, Environ Sci Technol, 48, 14386-14391, 10.1021/es504163z, 2014.

Lu, K. D., Hofzumahaus, A., Holland, F., Bohn, B., Brauers, T., Fuchs, H., Hu, M., Häseler, R., Kita, K., Kondo, Y., Li, X., Lou, S. R., Oebel, A., Shao, M., Zeng, L. M., Wahner, A., Zhu, T., Zhang, Y. H., and Rohrer, F.: Missing OH source in a suburban environment near Beijing: observed and modelled OH and HO_2 concentrations in summer 2006, Atmos. Chem. Phys., 13, 1057-1080, 10.5194/acp-13-1057-2013, 2013.

Makkonen, U., Virkkula, A., M¨antykentt¨a, J., Hakola, H., Keronen, P., Vakkari, V., and Aalto, P. P.: Semi-continuous gas and inorganic aerosol measurements at a Finnish urban site: comparisons with filters, nitrogen in aerosol and gas phases, and aerosol acidity, Atmos. Chem. Phys., 12, 5617–5631, 10.5194/acp-12-5617-2012, 2012.

McFall, A. S., Edwards, K. C., and Anastasio, C.: Nitrate Photochemistry at the Air-Ice Interface and in Other Ice Reservoirs, Environ. Sci. Technol., 52, 5710-5717, 10.1021/acs.est.8b00095, 2018.

Meusel, H., Kuhn, U., Reiffs, A., Mallik, C., Harder, H., Martinez, M., Schuladen, J., Bohn, B., Parchatka, U., Crowley, J. N., Fischer, H., Tomsche, L., Novelli, A., Hoffmann, T., Janssen, R. H. H., Hartogensis, O., Pikridas, M., Vrekoussis, M., Bourtsoukidis, E., Weber, B.,

689 Lelieveld, J., Williams, J., Poschl, U., Cheng, Y. F., and Su, H.: Daytime formation of nitrous acid at a coastal remote site in Cyprus
690 indicating a common ground source of atmospheric HONO and NO, Atmos. Chem. Phys., 16, 14475-14493, 10.5194/acp-16-14475-2016,
691 2016.

692 Michoud, V., Colomb, A., Borbon, A., Miet, K., Beekmann, M., Camredon, M., Aumont, B., Perrier, S., Zapf, P., Siour, G., Ait-Helal, W.,
693 Afif, C., Kukui, A., Furger, M., Dupont, J. C., Haeffelin, M., and Doussin, J. F.: Study of the unknown HONO daytime source at a
694 European suburban site during the MEGAPOLI summer and winter field campaigns, Atmos. Chem. Phys., 14, 2805-2822, 10.5194/acp-
695 14-2805-2014, 2014.

696 Min, K. E., Washenfelder, R. A., Dubé, W. P., Langford, A. O., Edwards, P. M., Zarzana, K. J., Stutz, J., Lu, K., Rohrer, F., Zhang, Y.,
697 and Brown, S. S.: A broadband cavity enhanced absorption spectrometer for aircraft measurements of glyoxal, methylglyoxal, nitrous acid,
698 nitrogen dioxide, and water vapor, Atmos. Meas. Tech., 9, 423-440, 10.5194/amt-9-423-2016, 2016.

699 Monge, M. E., D'Anna, B., Mazri, L., Giroir-Fendler, A., Ammann, M., Donaldson, D. J., and George, C.: Light changes the atmospheric
700 reactivity of soot, Proc Natl Acad Sci U S A, 107, 6605-6609, 10.1073/pnas.0908341107, 2010.

701 Ndour, M., D'Anna, B., George, C., Ka, O., Balkanski, Y., Kleffmann, J., Stemmler, K., and Ammann, M.: Photoenhanced uptake of NO_2
702 on mineral dust: Laboratory experiments and model simulations, Geophys. Res. Lett., 35, 10.1029/2007gl032006, 2008.

703 Nie, W., Ding, A. J., Xie, Y. N., Xu, Z., Mao, H., Kerminen, V.-M., Zheng, L. F., Qi, X. M., Huang, X., Yang, X.-Q., Sun, J. N.,
704 Herrmann, E., Petäjä, T., Kulmala, M., and Fu, C. B.: Influence of biomass burning plumes on HONO chemistry in eastern China, Atmos.
705 Chem. Phys., 15 1147–1159, 10.5194/acp-15-1147-2015, 2015a.

706 Nie, W., Ding, A. J., Xie, Y. N., Xu, Z., Mao, H., Kerminen, V. M., Zheng, L. F., Qi, X. M., Huang, X., Yang, X. Q., Sun, J. N., Herrmann,
707 E., Petäjä, T., Kulmala, M., and Fu, C. B.: Influence of biomass burning plumes on HONO chemistry in eastern China, Atmos. Chem.
708 Phys., 15, 1147-1159, 10.5194/acp-15-1147-2015, 2015b.

709 Oswald, R., Behrendt, T., Ermel, M., Wu, D., Su, H., Cheng, Y., Breuninger, C., Moravek, A., Mougin, E., Delon, C., Loubet, B.,
710 Pommerening-Roser, A., Sorgel, M., Poschl, U., Hoffmann, T., Andreae, M. O., Meixner, F. X., and Trebs, I.: HONO emissions from soil
711 bacteria as a major source of atmospheric reactive nitrogen, Science, 341, 1233-1235, 10.1126/science.1242266, 2013.

712 Park, S. S., Hong, S. B., Jung, Y. G., and Lee, J. H.: Measurements of PM_{10} aerosol and gas-phase nitrous acid during fall season in a
713 semi-urban atmosphere, Atmos. Environ., 38, 293-304, 10.1016/j.atmosenv.2003.09.041, 2004.

714 Perner, D. and Platt, U.: Detection of nitrous acid in the atmosphere by differential optical absorption, Geophys. Res. Lett., 6, 917-920,
715 doi:10.1029/GL006i012p00917, 1979.

716 Qin, M., Xie, P., Su, H., Gu, J., Peng, F., Li, S., Zeng, L., Liu, J., Liu, W., and Zhang, Y.: An observational study of the HONO–NO_2
717 coupling at an urban site in Guangzhou City, South China, Atmos. Environ., 43, 5731-5742, 10.1016/j.atmosenv.2009.08.017, 2009.

718 Rappenglück, B., Lubertino, G., Alvarez, S., Golovko, J., Czader, B., and Ackermann, L.: Radical precursors and related species from
719 traffic as observed and modeled at an urban highway junction, J. Air Waste Manage. Assoc., 63, 1270-1286,
720 10.1080/10962247.2013.822438, 2013.

721 Röckmann, T., Walter, S., Bohn, B., Wegener, R., Spahn, H., Brauers, T., Tillmann, R., Schlosser, E., Koppmann, R., and Rohrer, F.:
722 Isotope effect in the formation of H_2 from H_2CO studied at the atmospheric simulation chamber SAPHIR, Atmos. Chem. Phys., 10, 5343-
723 5357, 10.5194/acp-10-5343-2010, 2010.

724 Romer, P. S., Wooldridge, P. J., Crounse, J. D., Kim, M. J., Wennberg, P. O., Dibb, J. E., Scheuer, E., Blake, D. R., Meinardi, S., Brosius,
725 A. L., Thames, A. B., Miller, D. O., Brune, W. H., Hall, S. R., Ryerson, T. B., and Cohen, R. C.: Constraints on Aerosol Nitrate Photolysis
726 as a Potential Source of HONO and NO*x*, Environ. Sci. Technol., 10.1021/acs.est.8b03861, 2018.

727 Ryan, R. G., Rhodes, S., Tully, M., Wilson, S., Jones, N., Frieß, U., and Schofield, R.: Daytime HONO, NO_2 and aerosol distributions
728 from MAX-DOAS observations in Melbourne, Atmos. Chem. Phys. Discuss., 1-27, 10.5194/acp-2018-409, 2018.

729 Scharko, N. K., Berke, A. E., and Raff, J. D.: Release of Nitrous Acid and Nitrogen Dioxide from Nitrate Photolysis in Acidic Aqueous
730 Solutions, Environ. Sci. Technol. , 48, 11991-12001, 10.1021/es503088x, 2014.

731 Seinfeld, J. H. and Pandis, S. N.: Atmospheric Chemistry and Physics. From Air Pollution to Climate Changes, 1998.

732 Shi, X., Ge, Y., Zheng, J., Ma, Y., Ren, X., and Zhang, Y.: Budget of nitrous acid and its impacts on atmospheric oxidative capacity at an
733 urban site in the central Yangtze River Delta region of China, Atmospheric Environment, 238, 117725, 10.1016/j.atmosenv.2020.117725,
734 2020.

https://doi.org/10.5194/acp-2021-723
Preprint. Discussion started: 23 September 2021

Atmospheric Chemistry and Physics Discussions

735 Slanina, J., ten Brink, H. M., Otjes, R. P., Even, A., Jongejan, P., Khlystov, A., WaijersIjpelaan, A., and Hu, M.: The continuous analysis
736 of nitrate and ammonium in aerosols by the steam jet aerosol collector (SJAC): extension and validation of the methodology, Atmos.
737 Environ., 35, 2319-2330, 2001.

738 Sörgel, M., Regelin, E., Bozem, H., Diesch, J. M., Drewnick, F., Fischer, H., Harder, H., Held, A., Hosaynali-Beygi, Z., Martinez, M., and
739 Zetzsch, C.: Quantification of the unknown HONO daytime source and its relation to NO_2, Atmos. Chem. Phys., 11, 10433-10447,
740 10.5194/acp-11-10433-2011, 2011a.

741 Sörgel, M., Regelin, E., Bozem, H., Diesch, J. M., Drewnick, F., Fischer, H., Harder, H., Held, A., Hosaynali-Beygi, Z., Martinez, M., and
742 Zetzsch, C.: Quantification of the unknown HONO daytime source and its relation to NO_2, Atmos. Chem. Phys., 11, 10433-10447,
743 10.5194/acp-11-10433-2011, 2011b.

744 Spataro, F., Ianniello, A., Esposito, G., Allegrini, I., Zhu, T., and Hu, M.: Occurrence of atmospheric nitrous acid in the urban area of
745 Beijing (China), Sci. Total Environ., 447, 210-224, 10.1016/j.scitotenv.2012.12.065, 2013.

746 Stemmler, K., Ammann, M., Donders, C., Kleffmann, J., and George, C.: Photosensitized reduction of nitrogen dioxide on humic acid as a
747 source of nitrous acid, Nature, 440, 195-198, 10.1038/nature04603, 2006.

748 Stutz, J., Alicke, B., Ackermann, R., Geyer, A., Wang, S., White, A. B., Williams, E. J., Spicer, C. W., and Fast, J. D.: Relative humidity
749 dependence of HONO chemistry in urban areas, J. Geophys. Res. Atmos., 109, n/a-n/a, 10.1029/2003jd004135, 2004.

750 Su, H., Cheng, Y. F., Shao, M., Gao, D. F., Yu, Z. Y., Zeng, L. M., Slanina, J., Zhang, Y. H., and Wiedensohler, A.: Nitrous acid (HONO)
751 and its daytime sources at a rural site during the 2004 PRIDE-PRD experiment in China, J. Geophys. Res., 113, 10.1029/2007jd009060,
752 2008a.

753 Su, H., Cheng, Y. F., Shao, M., Gao, D. F., Yu, Z. Y., Zeng, L. M., Slanina, J., Zhang, Y. H., and Wiedensohler, A.: Nitrous acid (HONO)
754 and its daytime sources at a rural site during the 2004 PRIDE-PRD experiment in China, J. Geophys. Res., 113, 10.1029/2007jd009060,
755 2008b.

756 Su, H., Cheng, Y., Oswald, R., Behrendt, T., Trebs, I., Meixner, F. X., Andreae, M. O., Cheng, P., Zhang, Y., and Pöschl, U.: Soil nitrite
757 as a source of atmospheric HONO and OH radicals, Science, 333, 1616-1618, 2011.

758 Su, H., Cheng, Y. F., Cheng, P., Zhang, Y. H., Dong, S., Zeng, L. M., Wang, X., Slanina, J., Shao, M., and Wiedensohler, A.: Observation
759 of nighttime nitrous acid (HONO) formation at a non-urban site during PRIDE-PRD2004 in China, Atmos. Environ., 42, 6219-6232,
760 10.1016/j.atmosenv.2008.04.006, 2008c.

761 Tan, Z., Fuchs, H., Lu, K., Hofzumahaus, A., Bohn, B., Broch, S., Dong, H., Gomm, S., Häseler, R., He, L., Holland, F., Li, X., Liu, Y.,
762 Lu, S., Rohrer, F., Shao, M., Wang, B., Wang, M., Wu, Y., Zeng, L., Zhang, Y., Wahner, A., and Zhang, Y.: Radical chemistry at a rural
763 site (Wangdu) in the North China Plain: observation and model calculations of OH, HO_2 and RO_2 radicals, Atmos. Chem. Phys., 17, 663-
764 690, 10.5194/acp-17-663-2017, 2017.

765 Tang, K., Qin, M., Duan, J., Fang, W., Meng, F., Liang, S., Xie, P., Liu, J., Liu, W., Xue, C., and Mu, Y.: A dual dynamic chamber system
766 based on IBBCEAS for measuring fluxes of nitrous acid in agricultural fields in the North China Plain, Atmos. Environ., 196, 10-19,
767 10.1016/j.atmosenv.2018.09.059, 2019.

768 Underwood, G. M., Song, C. H., Phadnis, M., Carmichael, G. R., and Grassian, V. H.: Heterogeneous reactions of NO2and HNO3on
769 oxides and mineral dust: A combined laboratory and modeling study, J. Geophys. Res. Atmos., 106, 18055-18066, 10.1029/2000jd900552,
770 2001.

771 VandenBoer, T. C., Young, C. J., Talukdar, R. K., Markovic, M. Z., Brown, S. S., Roberts, J. M., and Murphy, J. G.: Nocturnal loss and
772 daytime source of nitrous acid through reactive uptake and displacement, Nat. Geosci., 8, 55-60, 10.1038/ngeo2298, 2014.

773 VandenBoer, T. C., Brown, S. S., Murphy, J. G., Keene, W. C., Young, C. J., Pszenny, A. A. P., Kim, S., Warneke, C., de Gouw, J. A.,
774 Maben, J. R., Wagner, N. L., Riedel, T. P., Thornton, J. A., Wolfe, D. E., Dubé, W. P., Öztürk, F., Brock, C. A., Grossberg, N., Lefer, B.,
775 Lerner, B., Middlebrook, A. M., and Roberts, J. M.: Understanding the role of the ground surface in HONO vertical structure: High
776 resolution vertical profiles during NACHTT-11, Journal of Geophysical Research: Atmospheres, 118, 10,155-110,171,
777 10.1002/jgrd.50721, 2013.

778 Villena, G., Bejan, I., Kurtenbach, R., Wiesen, P., and Kleffmann, J.: Interferences of commercial NO_2 instruments in the urban
779 atmosphere and in a smog chamber, Atmos. Meas. Techn., 5, 149-159, 10.5194/amt-5-149-2012, 2012.

780 Wagner, N. L., Riedel, T. P., Roberts, J. M., Thornton, J. A., Angevine, W. M., Williams, E. J., Lerner, B. M., Vlasenko, A., Li, S. M.,
781 Dubé, W. P., Coffman, D. J., Bon, D. M., de Gouw, J. A., Kuster, W. C., Gilman, J. B., and Brown, S. S.: The sea breeze/land breeze

circulation in Los Angeles and its influence on nitryl chloride production in this region, J. Geophys. Res. Atmos. , 117, n/a-n/a, 10.1029/2012jd017810, 2012.

Wang, H., Lyu, X., Guo, H., Wang, Y., Zou, S., Ling, Z., Wang, X., Jiang, F., Zeren, Y., Pan, W., Huang, X., and Shen, J.: Ozone pollution around a coastal region of South China Sea: interaction between marine and continental air, Atmos. Chem. Phys., 18, 4277–4295, 10.5194/acp-18-4277-2018, 2018.

Wang, J., Zhang, X., Guo, J., Wang, Z., and Zhang, M.: Observation of nitrous acid (HONO) in Beijing, China: Seasonal variation, nocturnal formation and daytime budget, Sci. Total Environ., 587-588, 350-359, 10.1016/j.scitotenv.2017.02.159, 2017.

Wang, L., Wen, L., Xu, C., Chen, J., Wang, X., Yang, L., Wang, W., Yang, X., Sui, X., Yao, L., and Zhang, Q.: HONO and its potential source particulate nitrite at an urban site in North China during the cold season, Sci. Total Environ., 538, 93-101, 10.1016/j.scitotenv.2015.08.032, 2015.

Wang, S.: Atmospheric observations of enhanced NO_2-HONO conversion on mineral dust particles, Geophys. Res. Lett., 30, 10.1029/2003gl017014, 2003.

Wang, S., Zhou, R., Zhao, H., Wang, Z., Chen, L., and Zhou, B.: Long-term observation of atmospheric nitrous acid (HONO) and its implication to local NO_2 levels in Shanghai, China, Atmos. Environ., 77, 718-724, 10.1016/j.atmosenv.2013.05.071, 2013.

Wen, L., Chen, T., Zheng, P., Wu, L., Wang, X., Mellouki, A., Xue, L., and Wang, W.: Nitrous acid in marine boundary layer over eastern Bohai Sea, China: Characteristics, sources, and implications, Sci. Total Environ., 10.1016/j.scitotenv.2019.03.225, 2019a.

Wen, L., Chen, T., Zheng, P., Wu, L., Wang, X., Mellouki, A., Xue, L., and Wang, W.: Nitrous acid in marine boundary layer over eastern Bohai Sea, China: Characteristics, sources, and implications, Sci. Total Environ., 670, 282-291, 10.1016/j.scitotenv.2019.03.225, 2019b.

Wong, K. W., Oh, H. J., Lefer, B. L., Rappenglück, B., and Stutz, J.: Vertical profiles of nitrous acid in the nocturnal urban atmosphere of Houston, TX, Atmos. Chem. Phys., 11, 3595-3609, 10.5194/acp-11-3595-2011, 2011.

Wyers, G. P., Oties, R. P., and Slanina, J.: A continuous-flow denuder for the measurement of ambient concentrations and surface-exchange fluxes of ammonia. , Atmos. Environ., 27, 2085-2090, 1993.

Xia, D., Zhang, X., Chen, J., Tong, S., Xie, H. B., Wang, Z., Xu, T., Ge, M., and Allen, D. T.: Heterogeneous Formation of HONO Catalyzed by CO_2, Environ. Sci. Technol., 10.1021/acs.est.1c02706, 2021.

Xu, W., Kuang, Y., Zhao, C., Tao, J., Zhao, G., Bian, Y., Yang, W., Yu, Y., Shen, C., Liang, L., Zhang, G., Lin, W., and Xu, X.: NH3-promoted hydrolysis of NO_2 induces explosive growth in HONO, Atmos. Chem. Phys., 19, 10557-10570, 10.5194/acp-19-10557-2019, 2019.

Xu, Z., Wang, T., Wu, J., Xue, L., Chan, J., Zha, Q., Zhou, S., Louie, P. K. K., and Luk, C. W. Y.: Nitrous acid (HONO) in a polluted subtropical atmosphere: Seasonal variability, direct vehicle emissions and heterogeneous production at ground surface, Atmos. Environ., 10.1016/j.atmosenv.2015.01.061, 2015.

Xun, A., huang, H., and Chen, D.: The observation and characteristic analysis of sea-land breeze circulation in Xiamen area, Straits Science, 12, 3-7, 2017.

Yabushita, A., Enami, S., Sakamoto, Y., Kawasaki, M., Hoffmann, M. R., and Colussi, A. J.: Anion-Catalyzed Dissolution of NO_2 on Aqueous Microdroplets, J. Phys. Chem. A, 113, 4844–4848, 2009.

Ye, C., Zhang, N., Gao, H., and Zhou, X.: Photolysis of Particulate Nitrate as a Source of HONO and NOx, Environ. Sci. Technol., 51, 6849-6856, 10.1021/acs.est.7b00387, 2017.

Ye, C., Zhou, X., Pu, D., Stutz, J., Festa, J., Spolaor, M., Tsai, C., Cantrell, C., Mauldin, R. L., 3rd, Campos, T., Weinheimer, A., Hornbrook, R. S., Apel, E. C., Guenther, A., Kaser, L., Yuan, B., Karl, T., Haggerty, J., Hall, S., Ullmann, K., Smith, J. N., Ortega, J., and Knote, C.: Rapid cycling of reactive nitrogen in the marine boundary layer, Nature, 532, 489-491, 10.1038/nature17195, 2016.

Yu, Y., Galle, B., Panday, A., Hodson, E., Prinn, R., and Wang, S.: Observations of high rates ofNO2-HONO conversion in the nocturnal atmospheric boundary layer in Kathmandu, Nepal, Atmos. Chem. Phys., 9 6401–6415, 2009.

Zhang, B. and Tao, F.-M.: Direct homogeneous nucleation of NO_2, H_2O, and NH_3 for the production of ammonium nitrate particles and HONO gas, Chem. Phys. Lett., 489, 143-147, 10.1016/j.cplett.2010.02.059, 2010.

https://doi.org/10.5194/acp-2021-723
Preprint. Discussion started: 23 September 2021

Atmospheric Chemistry and Physics Discussions

825 Zheng, J., Shi, X., Ma, Y., Ren, X., Jabbour, H., Diao, Y., Wang, W., Ge, Y., Zhang, Y., and Zhu, W.: Contribution of nitrous acid to the
826 atmospheric oxidation capacity in an industrial zone in the Yangtze River Delta region of China, Atmos. Chem. Phys., 20, 5457-5475,
827 10.5194/acp-20-5457-2020, 2020.

828 Zhou, L., Wang, W., Hou, S., Tong, S., and Ge, M.: Heterogeneous uptake of nitrogen dioxide on Chinese mineral dust, J Environ Sci
829 (China), 38, 110-118, 10.1016/j.jes.2015.05.017, 2015.

830 Zhou, X., Huang, G., Civerolo, K., Roychowdhury, U., and Demerjian, K. L.: Summertime observations of HONO, HCHO, and O_3 at the
831 summit of Whiteface Mountain, New York, J. Geophys. Res., 112, 10.1029/2006jd007256, 2007.

832 Zhou, X., Zhang, N., TerAvest, M., Tang, D., Hou, J., Bertman, S., Alaghmand, M., Shepson, P. B., Carroll, M. A., Griffith, S., Dusanter,
833 S., and Stevens, P. S.: Nitric acid photolysis on forest canopy surface as a source for tropospheric nitrous acid, Nat. Geosci., 4, 440-443,
834 10.1038/ngeo1164, 2011.

835

https://doi.org/10.5194/acp-2021-723
Preprint. Discussion started: 23 September 2021

Atmospheric Chemistry and Physics Discussions

Figure Captions

Figure 1. Location of Xiamen in China (left) and surroundings of IUE.

Figure 2. Time series of relative humidity (RH), temperature (T), J(HONO), UV, HONO, NO_2, NO, NO_3^-, $PM_{2.5}$, O_3, and black carbon (BC) in Xiamen, China in August, October, and December 2018, and March 2019. The missing data is mainly due to instrument maintenance.

Figure 3. Diurnal variations in HONO concentration on days with and without SLBs.

Figure 4. Diurnal variations in (a) HONO, (b) NO (hollow markers and dashed lines) & NOx (solid markers/lines), (c) HONO/NOx, and (d) $J(NO_2)$. The gray shading indicates nighttime (18:00–06:00, including 18:00).

Figure 5. Scatter plots of NO_2 versus HONO color coded by $J(NO_2)$. The three dashed lines represent 10 %, 5 %, and 1 % ratios of HONO/NO_2. Daytime was 06:00–18:00 LT, including 06:00.

Figure 6. Scatter plots of nighttime $HONO_{corr}/NO_2$ ratios versus RH. The average top-five $HONO_{corr}/NO_2$ in every 5 % RH interval are shown as orange squares, and the error bars show ±1 SD.

Figure 7. The correlation between the NH_3 concentration and HONO/NO_2 ratio (upper) and the correlation between the NH_3 concentration and the NO_3^-/NO_2 (lower) in four seasons. The scatter points were colored by ambient RH values.

Figure 8. The correlation between $PM_{2.5}$ and $HONO_{corr}$ (left) and the correlation between $PM_{2.5}$ and $HONO_{corr}/NO_2$ (right). The squares depict $PM_{2.5} \geq 35$ μg·m^{-3}; all scattered points are from the time when the ratio of $HONO_{corr}/NO_2$ reached a pseudo-steady state each night (03:00–06:00 LT).

Figure 9. Average diurnal variations of each source (>0) and sink (<0) of HONO in the four seasons.

Figure 10. Relationships between the photolysis of particulate nitrate and $R_{unknown}$, colored by BC in spring, summer, autumn, and winter. Red lines and dashed lines represent logarithmic fitting curve and turning point, respectively.

Figure 11. The ratio of HONO/NO_x in the four seasons (correlation between the average of NO_x per 10 ppb interval and the average value of HONO).

Figure 12. The diurnal variations in the measured values of HONO (black squares), the estimated values of HONO using the parameterized formula (red circles), and the estimated values of HONO using the parameterized formula combined with the main daytime sources (green triangles).

Figure 13. Comparison of OH formation by photolysis of HONO and O_3 in the four seasons.

https://doi.org/10.5194/acp-2021-723
Preprint. Discussion started: 23 September 2021

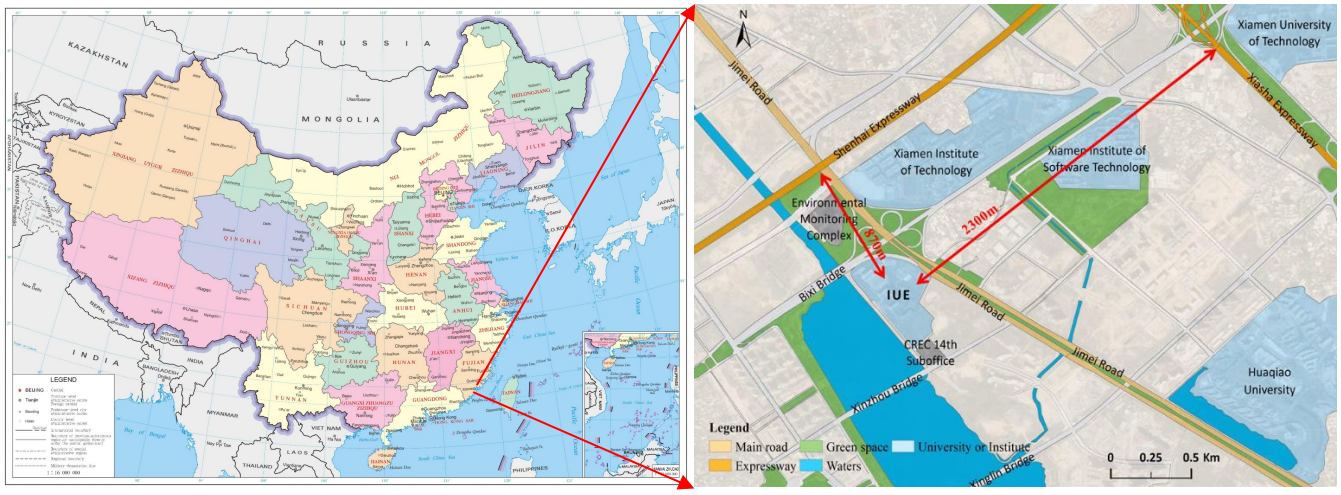

862

863 **Figure 1.** Location of Xiamen in China (left) and surroundings of IUE (right).

864 Note: The map in the left was directly download from http://bzdt.ch.mnr.gov.cn/, while the map in the right was significantly
865 enriched based on layer download from http://www.rivermap.cn/.

https://doi.org/10.5194/acp-2021-723
Preprint. Discussion started: 23 September 2021

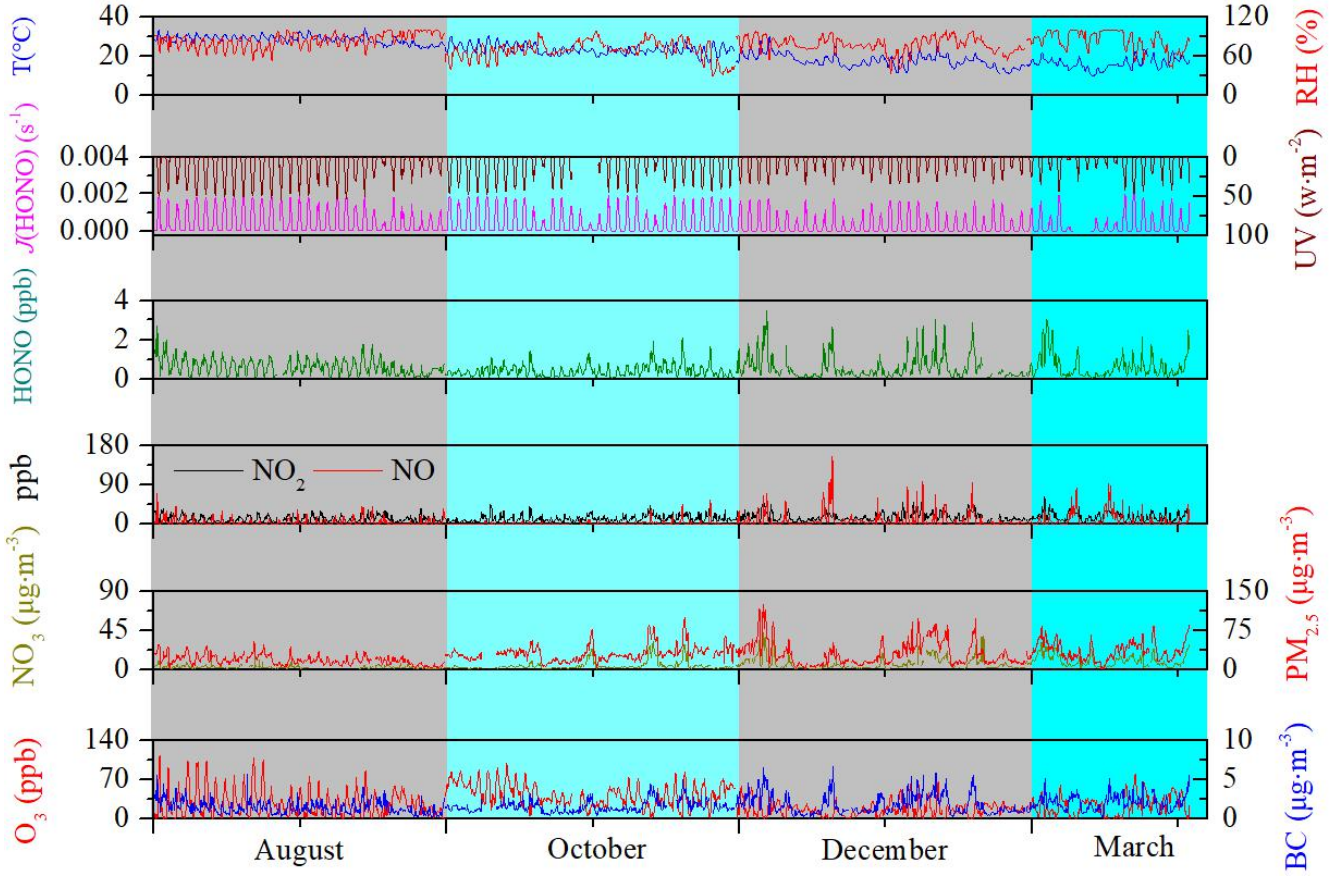

Figure 2. Time series of relative humidity (RH), temperature (T), *J*(HONO), UV, HONO, NO_2, NO, NO_3^-, $PM_{2.5}$, O_3, and black carbon (BC) in Xiamen, China in August, October, and December 2018, and March 2019. The missing data is mainly due to instrument maintenance.

https://doi.org/10.5194/acp-2021-723
Preprint. Discussion started: 23 September 2021

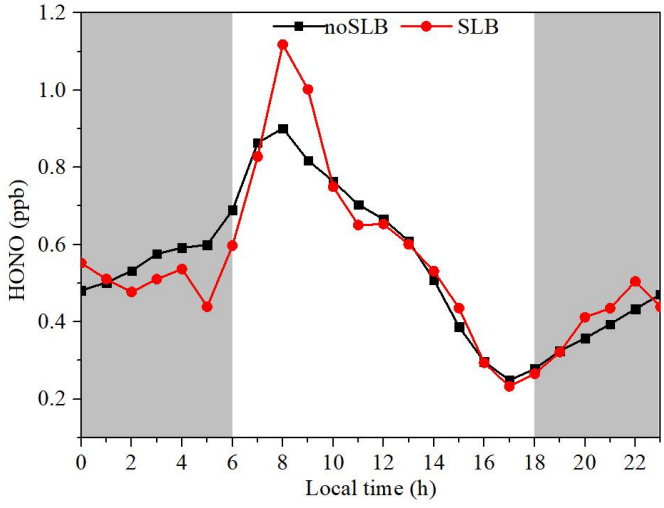

870

871 **Figure 3.** Diurnal variations in HONO concentration on days with and without SLBs.

https://doi.org/10.5194/acp-2021-723
Preprint. Discussion started: 23 September 2021

Atmospheric Chemistry and Physics Discussions

872

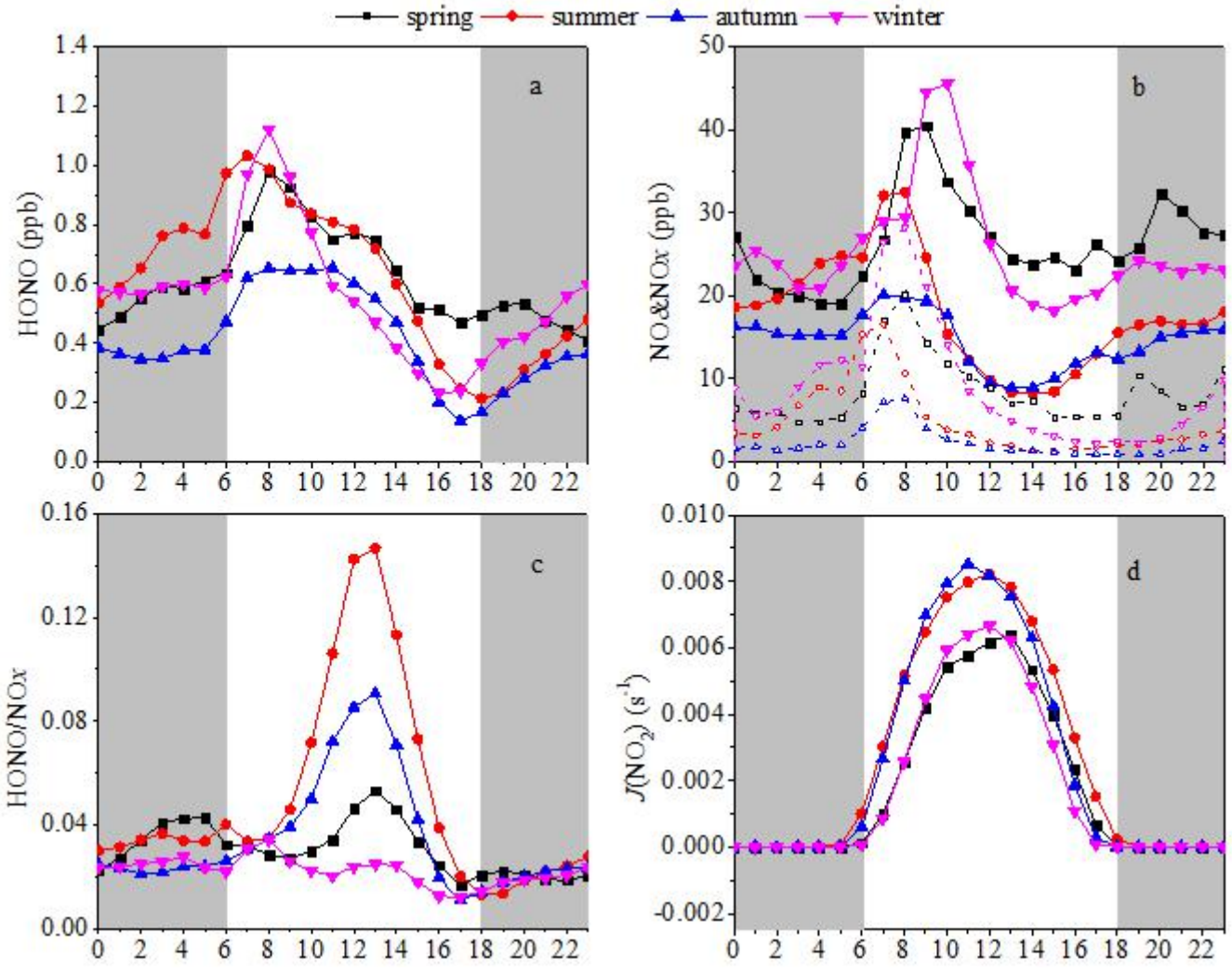

873

874 **Figure 4.** Diurnal variations in (a) HONO, (b) NO (hollow markers and dashed lines) & NO*x* (solid markers/lines), (c) HONO/NOx, and
875 (d) $J(NO_2)$. The gray shading indicates nighttime (18:00–06:00, including 18:00).

https://doi.org/10.5194/acp-2021-723
Preprint. Discussion started: 23 September 2021

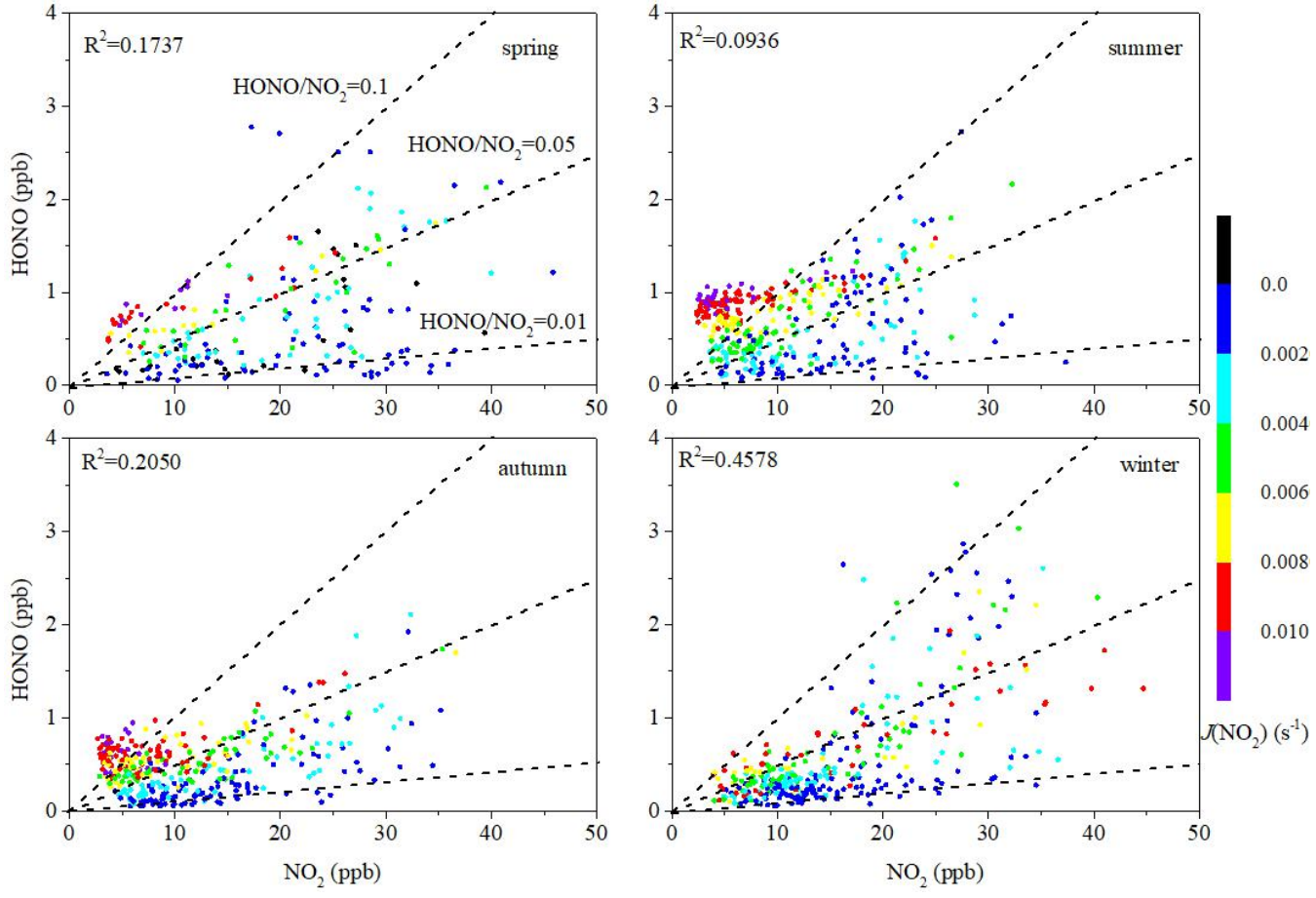

Figure 5. Scatter plots of NO_2 versus HONO color coded by $J(NO_2)$. The three dashed lines represent 10 %, 5 %, and 1 % ratios of $HONO/NO_2$. Daytime was 06:00–18:00 LT, including 06:00.

https://doi.org/10.5194/acp-2021-723
Preprint. Discussion started: 23 September 2021

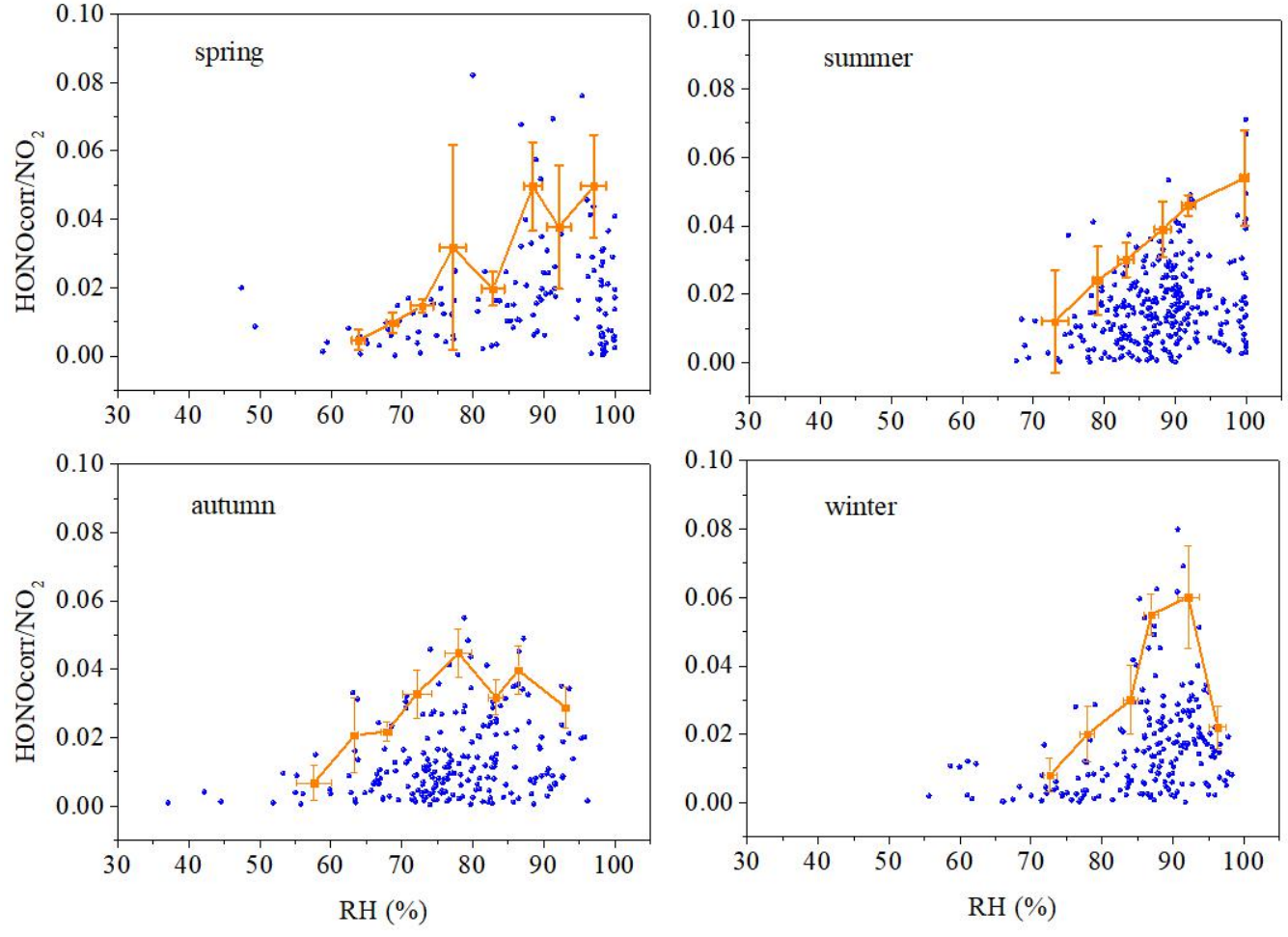

Figure 6. Scatter plots of nighttime $HONO_{corr}/NO_2$ ratios versus RH. The average top-five $HONO_{corr}/NO_2$ in every 5 % RH interval are shown as orange squares, and the error bars show ±1 SD.

https://doi.org/10.5194/acp-2021-723
Preprint. Discussion started: 23 September 2021

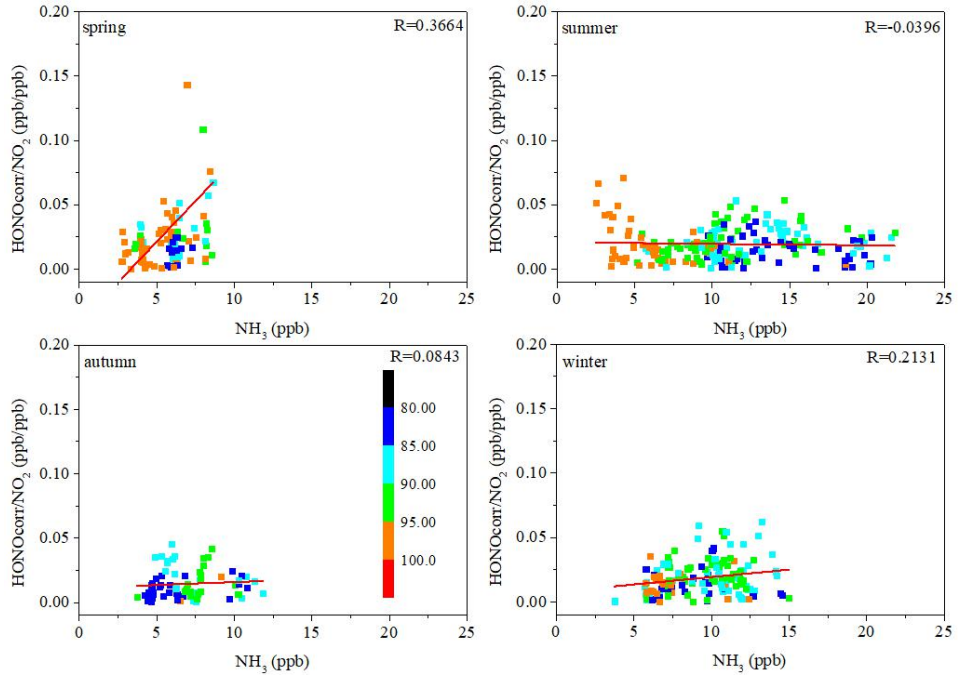

883

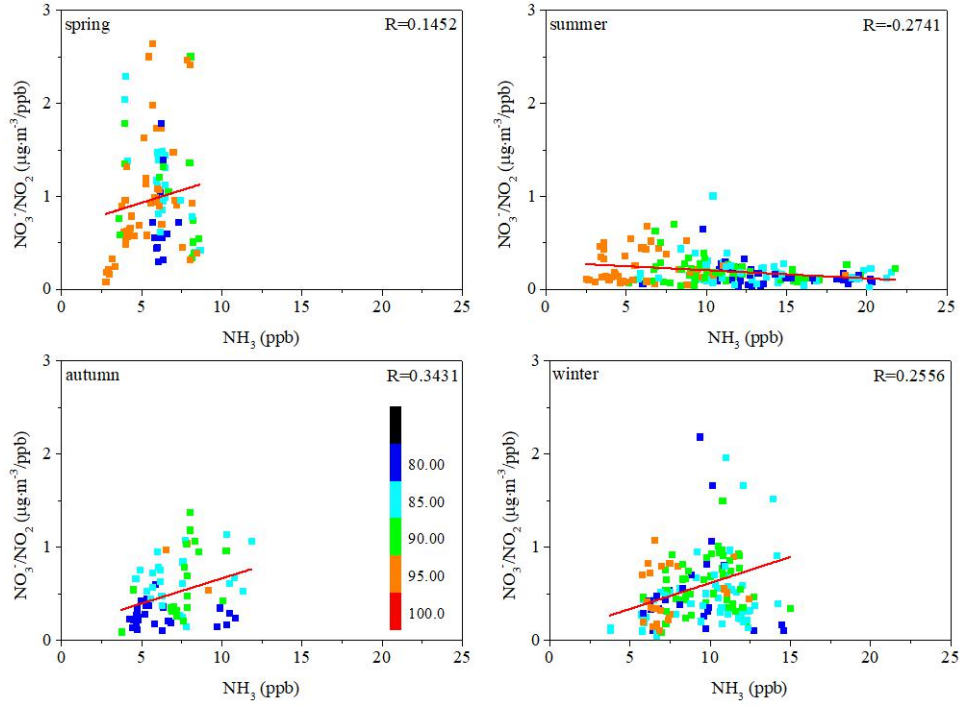

884

885 **Figure 7.** The correlation between the NH_3 concentration and $HONO/NO_2$ ratio (upper) and the correlation between the NH_3 concentration
886 and the NO_3^-/NO_2 (lower) in four seasons. The scatter points were colored by ambient RH values.

https://doi.org/10.5194/acp-2021-723
Preprint. Discussion started: 23 September 2021

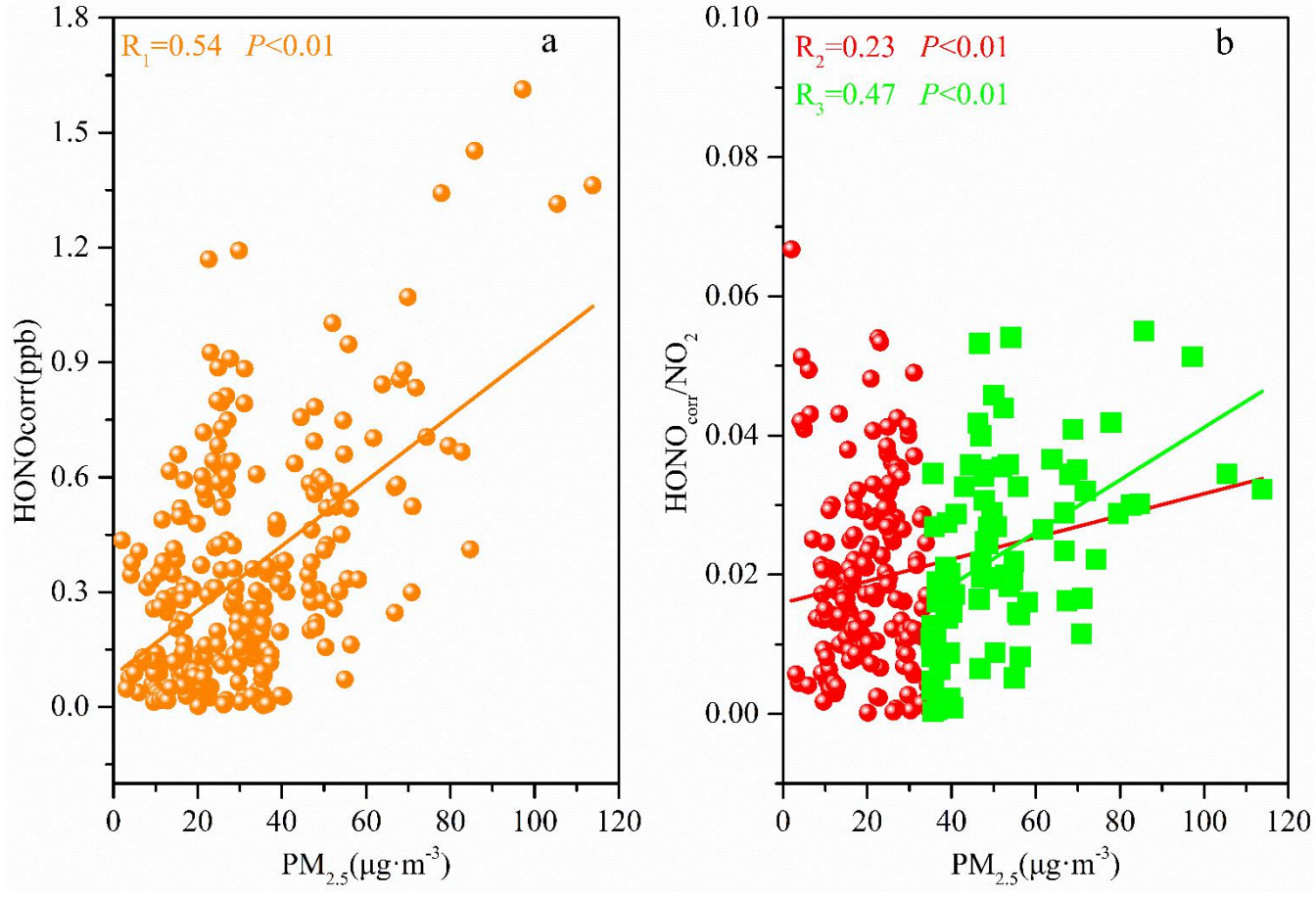

887

888 **Figure 8.** The correlation between $PM_{2.5}$ and $HONO_{corr}$ (left) and the correlation between $PM_{2.5}$ and $HONO_{corr}/NO_2$ (right). The squares
889 depict $PM_{2.5} \geq 35$ μg·m^{-3}; all scattered points are from the time when the ratio of $HONO_{corr}/NO_2$ reached a pseudo-steady state each night
890 (03:00–06:00 LT).

891

https://doi.org/10.5194/acp-2021-723
Preprint. Discussion started: 23 September 2021

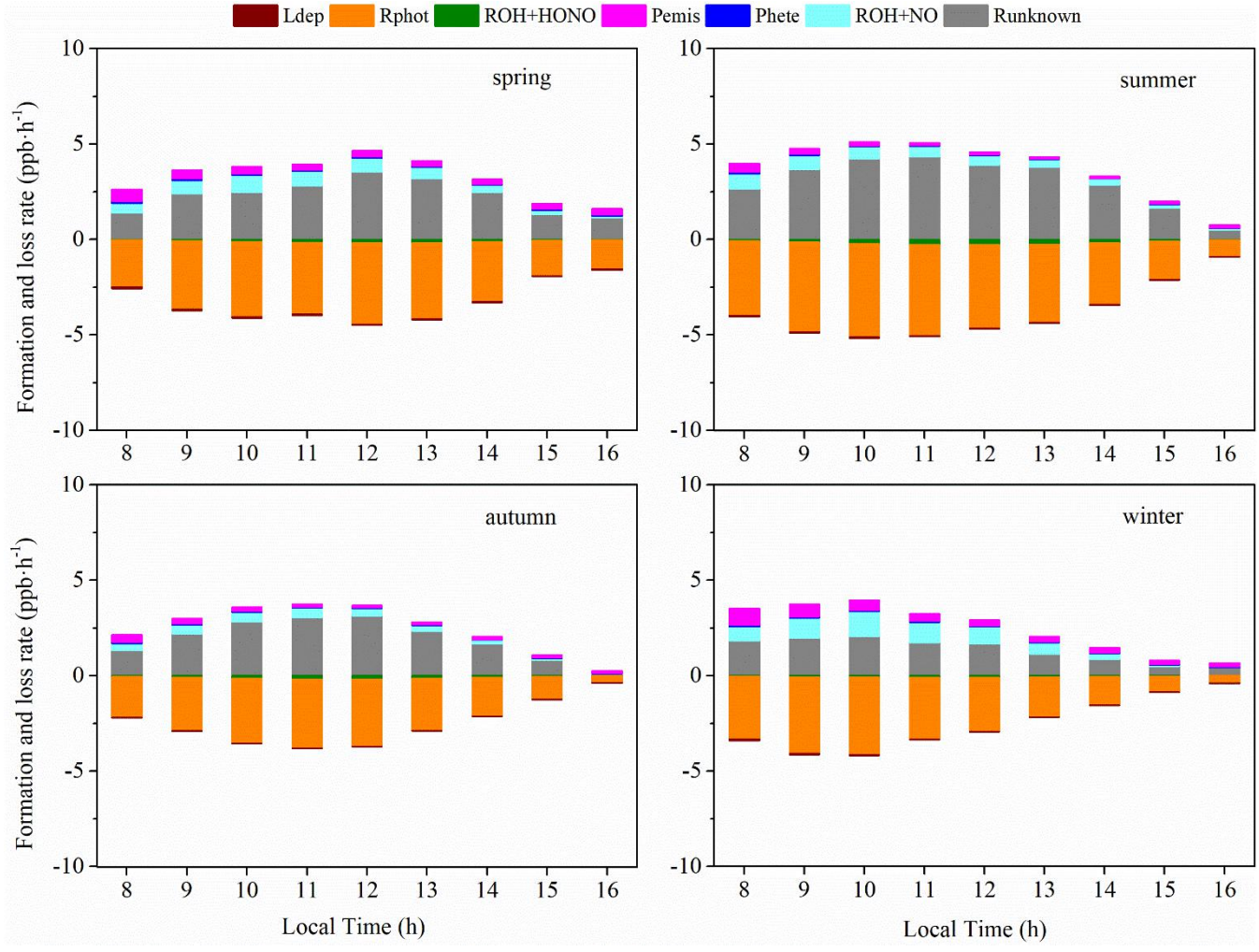

Figure 9. Average diurnal variations of each source (>0) and sink (<0) of HONO in the four seasons.

https://doi.org/10.5194/acp-2021-723
Preprint. Discussion started: 23 September 2021

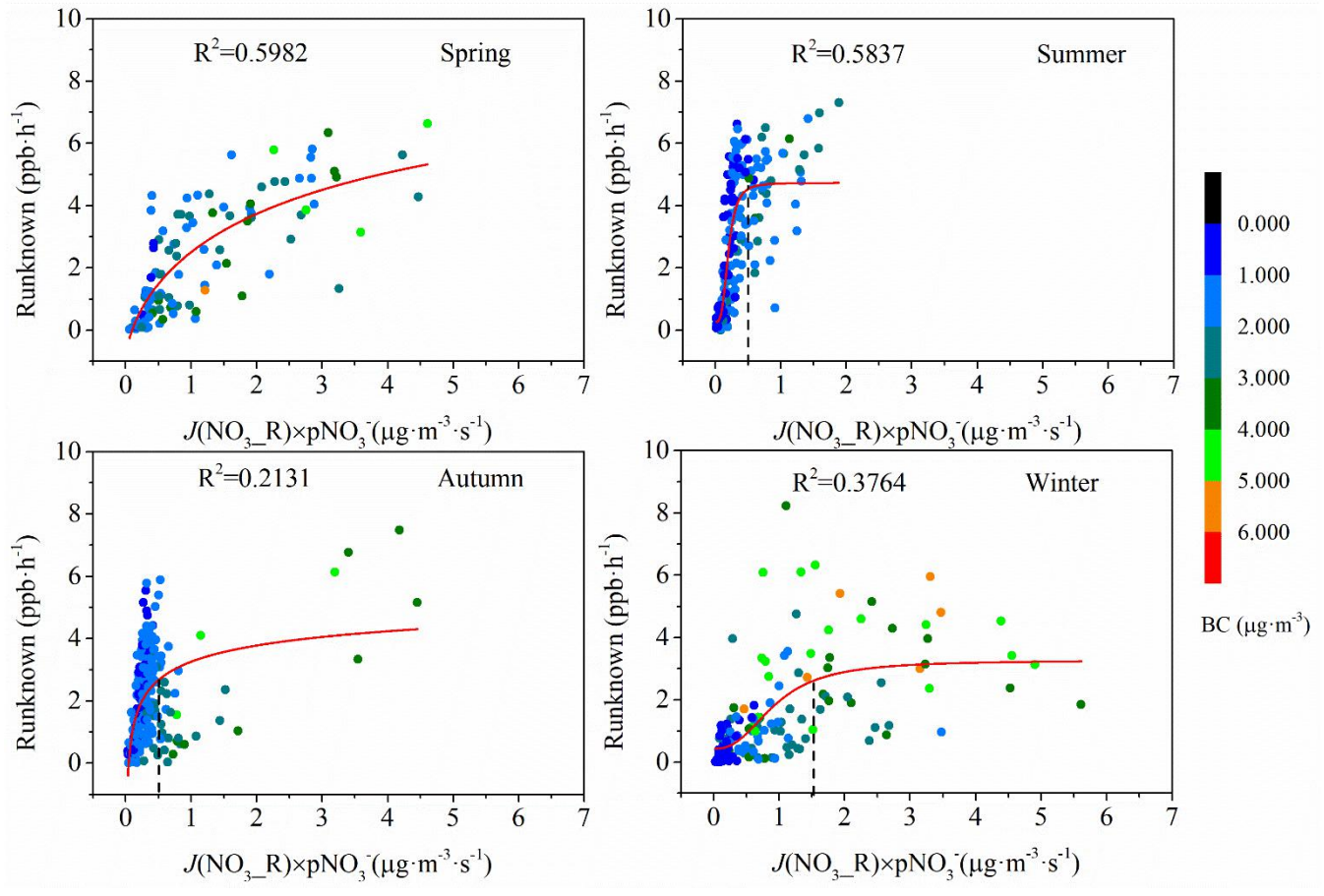

894

895 **Figure 10.** Relationships between the photolysis of particulate nitrate and $R_{unknown}$, colored by *BC* in spring, summer, autumn, and winter.
896 Red lines and dashed lines represent logarithmic fitting curve and turning point, respectively.

https://doi.org/10.5194/acp-2021-723
Preprint. Discussion started: 23 September 2021

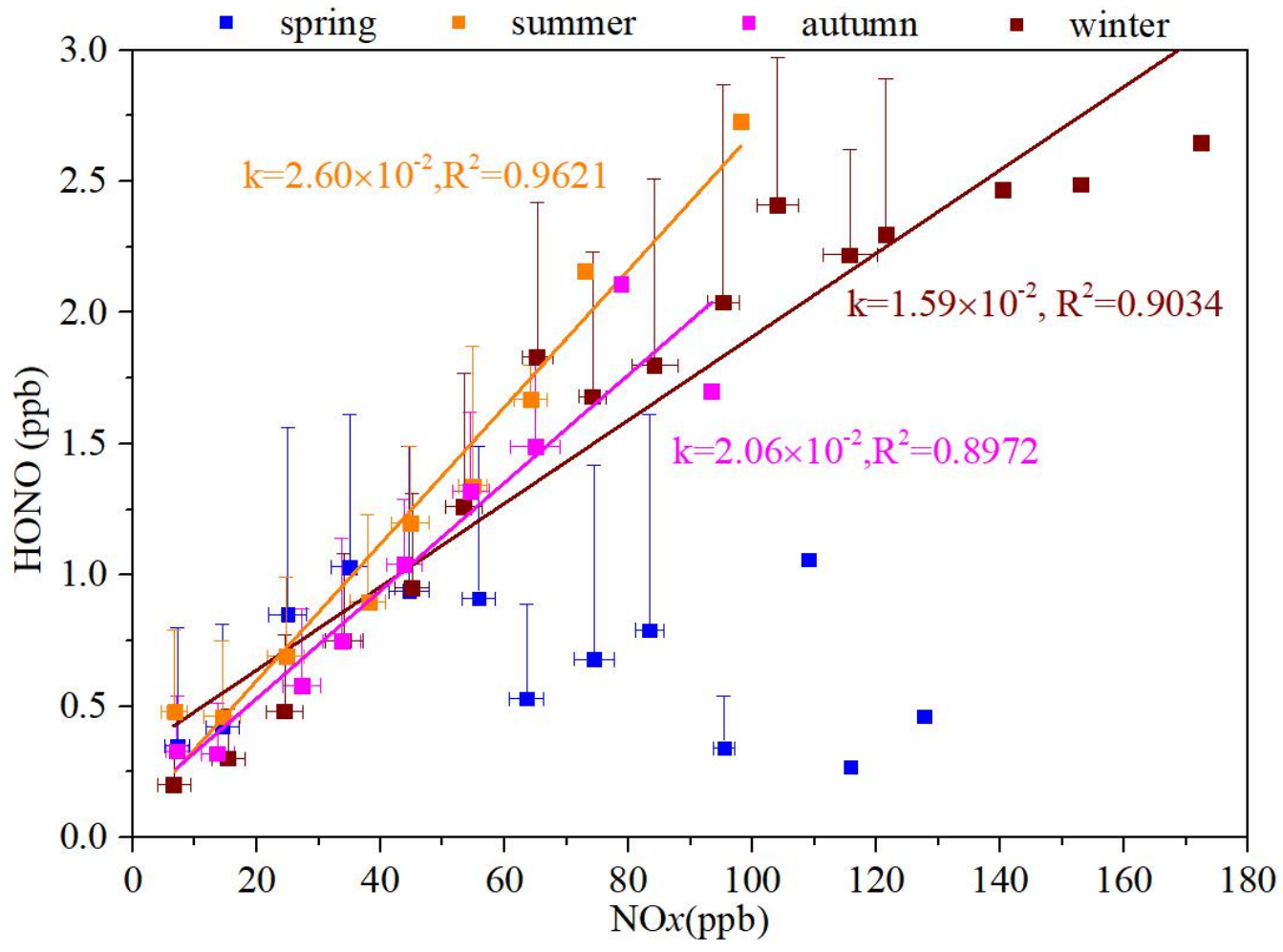

Figure 11. The ratio of HONO/NO_x in the four seasons (correlation between the average of NO_x per 10 ppb interval and the average value of HONO).

https://doi.org/10.5194/acp-2021-723
Preprint. Discussion started: 23 September 2021

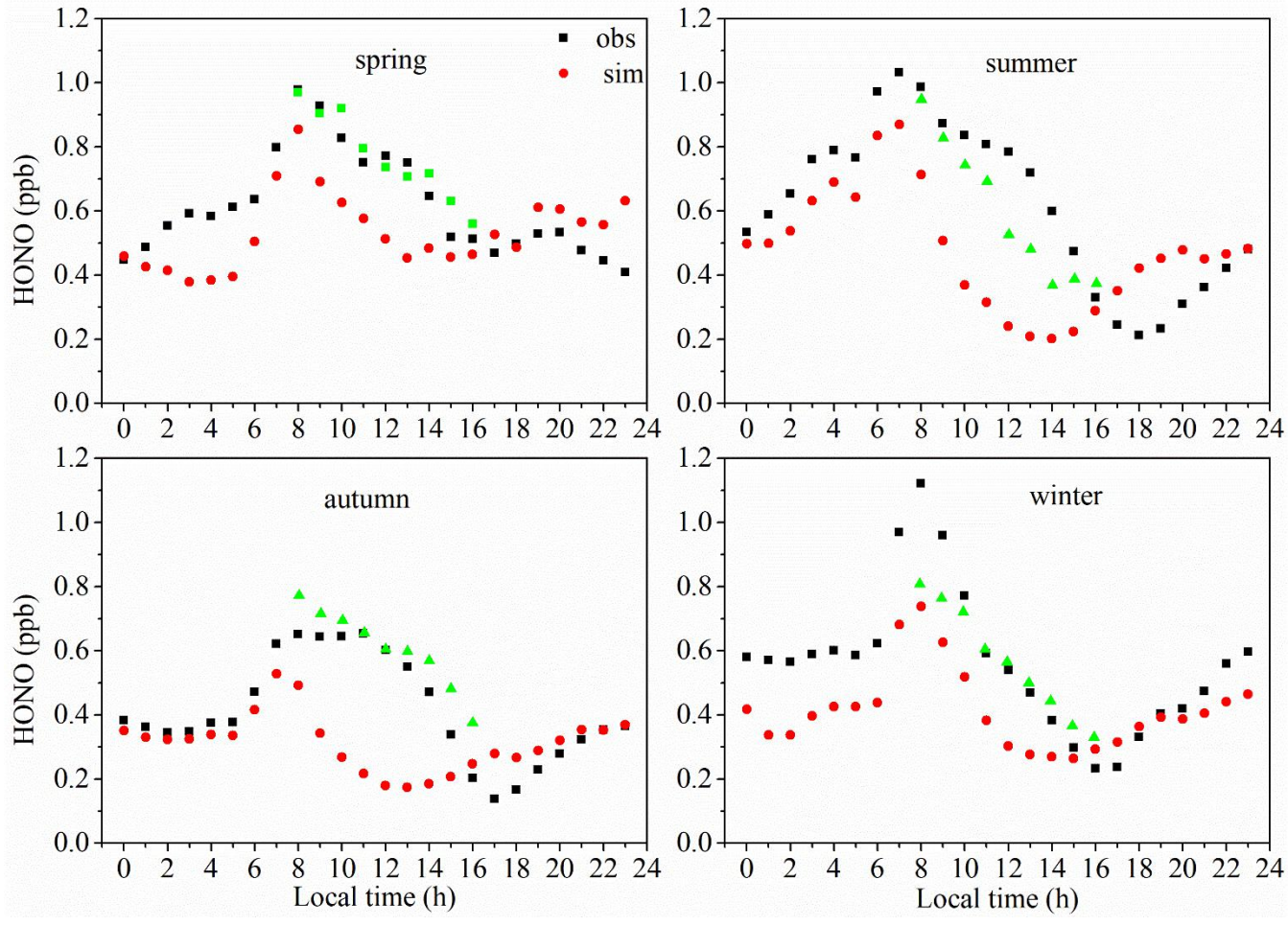

Figure 12. The diurnal variations in the measured values of HONO (black squares), the estimated values of HONO using the parameterized formula (red circles), and the estimated values of HONO using the parameterized formula combined with the main daytime sources (green triangles).

https://doi.org/10.5194/acp-2021-723
Preprint. Discussion started: 23 September 2021

Atmospheric Chemistry and Physics Discussions

904

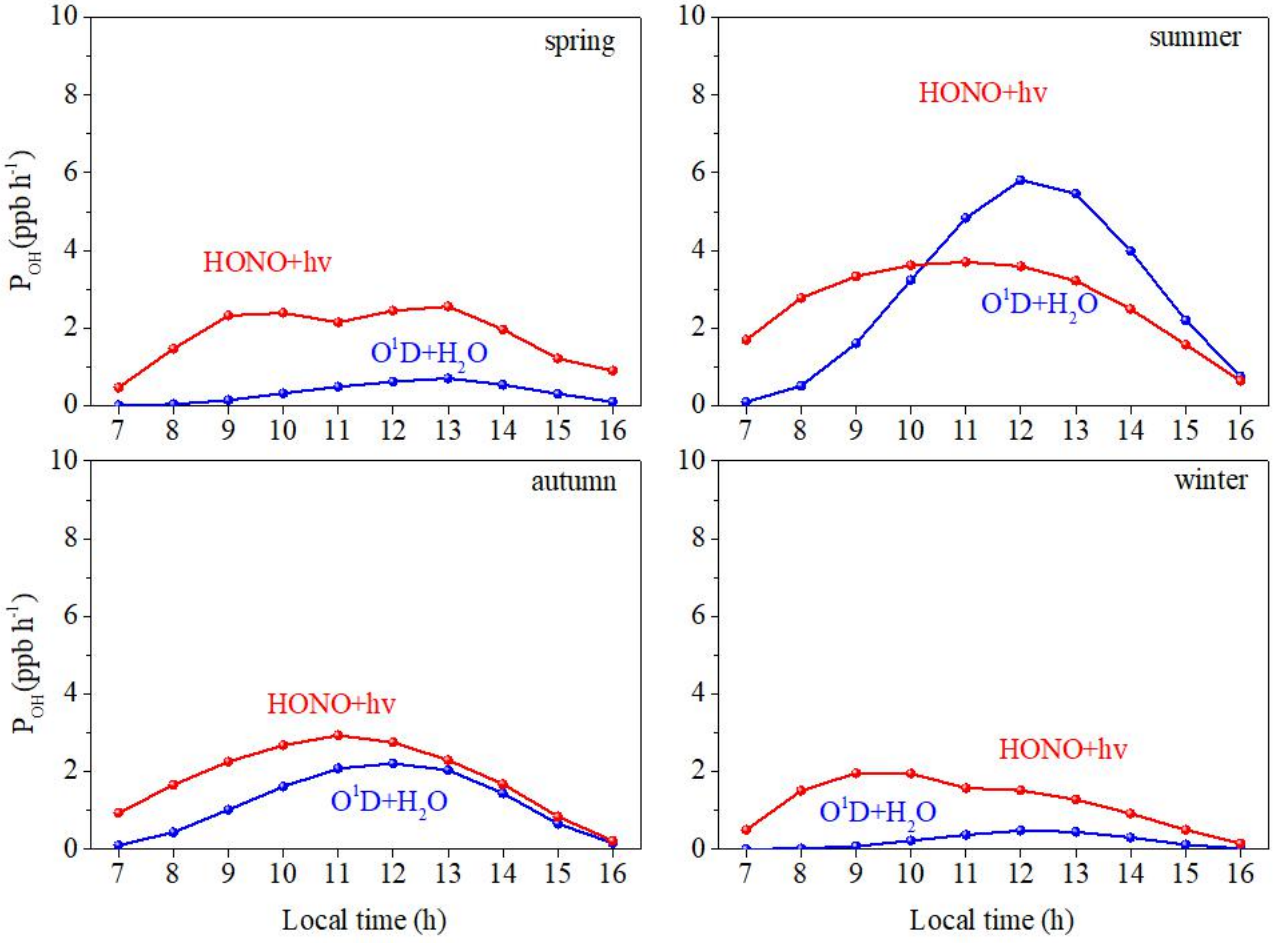

905

906 **Figure 13.** Comparison of OH formation by photolysis of HONO and O_3 in the four seasons.

907

https://doi.org/10.5194/acp-2021-723
Preprint. Discussion started: 23 September 2021

Atmospheric Chemistry and Physics Discussions

908 **Tables**

909 **Table 1.** Overview of the HONO and NO_x average concentrations measured in Xiamen and comparison with other
910 measurements.

911 **Table 2.** Emission ratios of fresh vehicle plumes $\Delta HONO/\Delta NO_x$.

912 **Table 3.** Overview of the conversion frequencies from NO_2 to HONO in Xiamen and comparisons with other studies.

https://doi.org/10.5194/acp-2021-723
Preprint. Discussion started: 23 September 2021

Atmospheric Chemistry and Physics Discussions

913 **Table 1.** Overview of the HONO and NO_x average concentrations measured in Xiamen and comparison with other
914 measurements.

Location	Date	HONO (ppb)		NO_2 (ppb)		NOx (ppb)		HONO/NO_2		HONO/NOx		Reference
		Day	Night	Day	Night	Day	Night	Day	Night	Day	Night	
Xiamen/China (suburban)	Aug.2018-Mar.2019	0.63	0.46	13.6	16.3	20.9	19.9	0.061	0.028	0.046	0.024	This work
	Mar.2019(spring)	0.72	0.51	18.5	17.7	28.6	24.5	0.046	0.032	0.034	0.028	
	Aug.2018(summer)	0.72	0.51	11.0	15.7	16.6	18.9	0.094	0.031	0.072	0.027	
	Oct.2018(autumn)	0.50	0.33	11.4	14.3	14.1	15.1	0.060	0.023	0.048	0.022	
	Dec.2018(winter)	0.61	0.52	15.8	18.3	28.0	23.1	0.036	0.026	0.023	0.022	
Jinan/China (urban)	Sep 2015-Aug 2016	0.99	1.28	25.8	31.0	40.6	46.4	0.056	0.079	0.035	0.040	(Li et al., 2018a)
	Sep.-Nov. 2015 (autumn)	0.66	0.87	23.2	25.4	37.5	38.0	0.034	0.049	0.022	0.034	
	Dec.2015-Feb.2016(winter)	1.35	2.15	34.6	41.1	64.8	78.5	0.047	0.056	0.031	0.034	
	Mar.-May 2016 (spring)	1.04	1.24	25.8	35.8	36.0	47.3	0.052	0.046	0.041	0.035	
	Jun.-Aug. 2016 (summer)	1.01	1.20	19.0	22.5	25.8	29.1	0.079	0.106	0.049	0.060	
Nanjing/China (suburban)	Nov. 2017-Nov. 2018	0.57	0.80	13.9	18.9	19.3	24.9	0.044	0.045	0.036	0.041	(Liu et al., 2019c)
	Dec.-Feb. (winter)	0.92	1.15	23.1	28.4	37.7	45.5	0.038	0.040	0.025	0.029	
	Mar.-May (spring)	0.59	0.76	12.9	17.4	15.9	19.1	0.049	0.048	0.042	0.046	
	Jun.-Aug. (summer)	0.34	0.56	7.7	12.5	9.1	13.5	0.051	0.048	0.045	0.046	
	Sep.-Nov. (autumn)	0.51	0.81	13.4	18.9	17.7	25.1	0.035	0.044	0.029	0.039	
Hongkong/China	Aug.2011(summer)	0.70	0.66	18.1	21.8	29.3	29.3	0.042	0.031	0.028	0.025	(Xu et al., 2015)
	Nov.2011(autumn)	0.89	0.95	29.0	27.2	40.6	37.2	0.030	0.034	0.021	0.028	
	Feb.2012(winter)	0.92	0.88	25.8	22.2	48.3	37.8	0.035	0.036	0.020	0.025	
	May2012(spring)	0.40	0.33	15.0	14.7	21.1	19.1	0.030	0.022	0.022	0.019	
Guangzhou/China (urban)	Jun.2006	2.00	3.50	30.0	20.0	-	-	0.067	0.175	-	-	(Qin et al., 2009)
Xi′an/China	Jul.-Aug.2015	1.57	0.51	24.7	15.4	-	-	0.062	0.033	-	-	(Huang et al., 2017)
Santiago/Chile (urban)	Mar.-Jun.2005	1.50	3.00	20.0	30.0	40.0	200.0	0.075	0.100	0.038	0.015	(Elshorbany et al., 2009)
Rome/Italy (urban)	May-Jun.2001	0.15	1.00	4.0	27.2	4.2	51.2	0.038	0.037	0.024	0.020	(Acker et al., 2006)
Kathmandu/Nepal (urban)	Jan.-Feb.2003	0.35	1.74	8.6	17.9	13.0	20.1	0.041	0.097	0.027	0.087	(Yu et al., 2009)

915 Note: Night (18:00-6:00, including 18:00, local time); Day (6:00-18:00, including 6:00, local time)

916 NOx=NO_2 (IBBCEAS)+NO (Thermal 42i). IBBCEAS measure both HONO and NO_2. The NO_2 concentration is always overestimated by
917 the Thermo Fisher 42i.

https://doi.org/10.5194/acp-2021-723
Preprint. Discussion started: 23 September 2021

Atmospheric Chemistry and Physics Discussions

Table 2. Emission ratios of fresh vehicle plumes ΔHONO/ΔNO*x*.

Date	Time	ΔNO/ΔNOx	R^2	ΔHONO/ΔNOx (%)
2018/8/1	7:00-8:55	1.1621	0.6897	2.17
2018/8/8	5:40-5:55	0.8727	0.8023	2.69
2018/8/21	5:00-5:55	0.8571	0.7553	1.14
2018/8/22	7:20-7:45	0.4998	0.6151	4.76
2018/8/23	5:20-5:55	0.7321	0.8089	2.12
2018/8/23	6:00-6:55	0.8321	0.6687	2.19
2018/8/31	23:35-23:55	1.1861	0.8130	1.18
2018/10/23	1:05-1:25	0.9893	0.6566	1.27
2018/12/4	7:20-7:40	0.9594	0.8502	1.11
2018/12/10	11:00-11:15	0.8778	0.6735	1.79
2018/12/11	0:00-0:50	0.9424	0.6972	0.58
2018/12/11	1:25-1:55	0.8492	0.8237	1.26
2018/12/11	2:50-3:55	0.7405	0.7520	2.87
2018/12/11	4:00-4:55	0.9652	0.7686	2.12
2018/12/11	5:45-6:35	1.0243	0.6566	0.84
2018/12/11	6:40-7:40	0.9992	0.7067	1.59
2018/12/11	8:15-8:55	0.8333	0.6820	1.89
2018/12/13	7:00-8:50	0.8263	0.8127	1.02
2018/12/13	9:10-9:45	0.7235	0.7776	1.01
2018/12/16	7:00-7:55	0.7523	0.8939	0.98
2018/12/18	7:35-8:10	0.7046	0.7110	1.15
2018/12/20	22:50-23:10	0.9811	0.7736	0.97
2018/12/21	0:45-1:15	1.0029	0.8914	1.54
2018/12/22	6:40-7:35	1.0194	0.7010	2.36
2018/12/22	7:40-8:05	0.9932	0.7831	2.94
2018/12/25	21:00-22:10	0.9573	0.8857	1.64
2018/12/26	3:50-4:15	1.167	0.6540	1.39
2018/12/26	6:45-7:45	0.9971	0.8463	0.92
2018/12/26	7:55-8:25	0.9714	0.6919	2.95
2018/12/27	4:50-5:30	0.9365	0.7265	0.76
2019/3/6	7:30-8:05	1.0309	0.8283	0.74
2019/3/9	7:50-8:05	0.9933	0.9203	0.24
2019/3/9	12:00-12:55	0.9627	0.6444	0.51
2019/3/18	6:35-8:35	1.0382	0.6967	3.14

https://doi.org/10.5194/acp-2021-723
Preprint. Discussion started: 23 September 2021

Atmospheric Chemistry and Physics Discussions

920 **Table 3.** Overview of the conversion frequencies from NO_2 to HONO in Xiamen and comparisons with other studies.

Location	Date	Conversion rate (% h-1)	Reference
Xiamen/China	Aug.2018-Mar.2019	0.47	This study
	Mar.2019(spring)	0.47	
	Aug.2018(summer)	0.55	
	Oct.2018(autumn)	0.48	
	Dec.2018(winter)	0.37	
Xinken/China	Oct.-Nov.,2004	1.60	(Su et al., 2008c)
Jinan/China	Sep.,2015-Aug.,2016	0.68	(Li et al., 2018a)
	Mar.-May 2016(spring)	0.43	
	Jun.-Aug. 2016(summer)	0.69	
	Sep.-Nov. 2015(autumn)	0.75	
	Dec.2015-Feb. 2016(winter)	0.83	
Guangzhou/China	Jun.,2006	2.40	(Li et al., 2012b)
Spain	Nov.-Dec.,2008	1.50	(Sörgel et al., 2011a)
Beijing/China	Sep.2015-July 2016	0.80	(Wang et al., 2017)
	Apr.-May, 2016 (spring)	0.50	
	Jun.-Jul., 2016 (summer)	1.00	
	Sep.-Oct. 2015 (autumn)	0.90	
	Jan.2016 (winter)	0.60	
Shandong/China	Nov.2013-Jan.2014	0.29	(Wang et al., 2015)
Shanghai/China	Aug.2010-Jun.2012	0.70	(Wang et al., 2013)
Eastern Bohai Sea/China	Oct.-Nov., 2016	1.80	(Wen et al., 2019a)
Hongkong/China	Aug.2011-May, 2012	0.52	(Xu et al., 2015)
Kathmandu/South Asia	Jan.-Feb.,2003	1.4	(Yu et al., 2009)

921